Correlation studies for the ^{7}He excited states

M. S. Khirk [1,2,3,*] L. V. Grigorenko [1,4,5] E. Yu. Nikolskii [1,5] and P. G. Sharov [1,6]

[1] *Flerov Laboratory of Nuclear Reactions, JINR, 141980 Dubna, Russia*

[2] *M.V. Lomonosov Moscow State University, Skobeltsyn Institute of Nuclear Physics, 119991 Moscow, Russia*

[3] *MIREA - Russian Technological University, 119454 Moscow, Russia*

[4] *National Research Nuclear University "MEPhI", 115409 Moscow, Russia*

[5] *National Research Centre "Kurchatov Institute", Kurchatov sq. 1, 123182 Moscow, Russia*

[6] *Institute of Physics, Silesian University in Opava, 74601 Opava, Czech Republic*

(Received 21 June 2025; accepted 12 September 2025; published 16 October 2025)

The unbound nucleus ^{7}He was recently studied in the ^{2}H(^{6}He, ^{1}H)^{7}He reaction at 29 A MeV beam energy by Golovkov *et al.* [Phys. Rev. C **109**, L061602 (2024)]. The excitation spectrum of ^{7}He was measured up to $E_T = 8$ MeV (E_T is energy above the ^{6}He -n threshold). Angular distribution for the ^{6}He -n decay of the ^{7}He $3/2^-$ ground state can be explained by a strong spin alignment induced by a reaction mechanism. The correlation information for the higher-lying ^{7}He excitations is available as backward-forward asymmetry for the ^{6}He -n decay in the ^{7}He frame. The asymmetry function has an expressed energy profile, which may be explained by using quite restrictive assumptions about structure of ^{7}He excitations or/and peculiarities of the reaction mechanism. In the analysis of Golovkov *et al.* the observation the $s_{1/2}$ state in ^{7}He is declared with $E_r \approx 2.0$ MeV. Our work is based on the same ^{7}He data. However, the data analysis was improved and also the data interpretation is substantiated with the detailed PWBA reaction studies and coupled-channel calculations of the ^{7}He continuous spectrum. The idea of the $s_{1/2}$ resonant state with $E_r \approx 2.0$ is rejected. In addition, the position of the $1/2^-$ state in ^{7}He is confined to the interval $E_r = 2.2$–3.0 MeV, with preferred value 2.6 MeV. There is indication on the second $3/2^-$ state in the data with $E_r \approx 4.5$ MeV and with the lower resonance energy limit $E_r \gtrsim 3.5$ MeV. Importance and prospects of more detailed correlation studies of ^{7}He continuum are discussed.

DOI: 10.1103/z2k7-tqwz

I. INTRODUCTION

Clear understanding of excitation spectra of the lightest nuclei is critical for general understanding of nuclear structure and nucleon-nucleon interaction in nuclei. The ^{7}He is intriguing system in this sense. We know the $3/2^-$ ground state (g.s.) properties very well. The $5/2^-$ state at $E_T \approx 3$ MeV above the ^{6}He -n threshold is clearly identified because of its unique dominating decay pattern ^{4}He $+3n$ [1]. However, information about other ^{7}He excitations is nebulous.

The ^{7}He continuum has already been studied in the (d, p) reaction [2,3]. In comparison with the previous works a more complex detector setup, which allows us to detect ^{7}He decay products (and, thus, makes possible correlation studies) was used in the experiment [4,5]. This work is based on the same ^{7}He data as Refs. [4,5], however, with improved analysis procedure and extensive theoretical discussion focused on correlation studies, see Secs. II and VII. The correlation data provide a distinctive rapid-varying behavior of the backward-forward asymmetry function for population of the ^{7}He continuum. Such a behavior of this function may be explained by using quite restrictive assumptions as it is strongly sensitive to the fine details of all the $3/2^-$, $1/2^-$, and $1/2^+$ configurations expected in the low-energy range of the ^{7}He spectrum.

Generally, the ^{7}He system has been studied many times and detailed reviews of this work can be found in Refs. [6] and [7]. There is the $3/2^-$ g.s. at $E_T = 0.445$ MeV and some broad overlapping structures are typically observed above it. The evident candidate to be present in this structures is the $1/2^-$ spin-orbit partner of the $3/2^-$ ground state. The review [7] split the results in this field into two camps: (i) the works that support existence of the low-lying $1/2^-$ excited state with $E \lesssim 2$ MeV in ^{7}He [8–15], and (ii) the works that are in favor of the $1/2^-$ with $E_T \gtrsim 2$ MeV [3,16–24]. Such a dichotomy is a bit artificial, however it well demonstrates a strong disagreement among different studies, both theoretical and experimental. The ^{6}He -n correlation data obtained in this work indicate that the $1/2^-$ state should be reasonably low-lying ($E_T \approx 2.2$–3.0 MeV) and should be well populated (with population cross section, comparable with the cross section for the $3/2^-$ g.s.).

The $3/2^-$ g.s. is well known to have non-single-particle structure with important (even dominant) ^{6}He$(2^+) + n$ wave function (WF) component. Qualitatively this means that the excited states represented by the orthogonal (to the g.s.) mixtures of the ^{6}He(g.s.)$+n$ and ^{6}He$(2^+) + n$ WF components may be situated reasonably low in excitation energy. There

*Contact author: mskhirk@jinr.ru

are various theoretical calculations predicting the $3/2^-_2$ state of ^{7}He at $E_T \approx 3.5$–6.0 MeV [24–26]. There is indication on the second $3/2^-_2$ state in our ^{7}He data with $E_r \approx 4.5$ MeV and with the lower resonance energy limit $E_r \gtrsim 3.5$ MeV.

We also discuss possibility of the resonant $1/2^+$ state at about $E_T \approx 2$–3 MeV as predicted in$E_T \approx 3.5$–6.0 [26] and observation of such a state in ^{7}He is declared in Ref. [5] with $E_r \approx 2.0$, $\Gamma \approx 2.0$ MeV. The possibility of the $1/2^+$ state in ^{9}He was for a long time discussed [27–30]. From qualitative point of view the principal possibility of such a state in ^{9}He is supported by evolution of the $s_{1/2}$ intruder orbital along the $N = 7$ isotone: there are ground states in ^{10}Li, ^{11}Be and low-lying excitations in ^{12}B, ^{13}C build on the $s_{1/2}$ configuration. No such support for the low-lying $1/2^+$ state of ^{7}He can be found in the $N = 5$ isotone: only in ^{9}Be there is a weak evidence for the $1/2^+$ state above the ^{8}Be $+n$ threshold. Theoretical works except the paper [26] all predict either no low-lying $1/2^+$ state or repulsion in the ^{6}He $+n$ channel [24,25,31–34]. In our work we demonstrate that the on-shell R-matrix parametrization used in Ref. [5] to infer the $1/2^+$ resonance properties in ^{7}He is not applicable for the reaction studies (where the off-shell T matrix should be applied).

The situation when we do not understand such a basic structure characteristic as spin-split between spin-orbit partners and the ground state multiplet structure in such a simple light nuclide as ^{7}He is quite unsatisfactory and it is calling to a dedicated research. So, the aim of this work is to get a deeper insight in these questions by using the correlation information obtained in the ^{2}H(^{6}He, ^{1}H) ^{7}He reaction.The system of units $\hbar = c = 1$ is used in this work.

II. EXPERIMENTAL SETUP AND METHOD

The experiment was carried out at the fragment separator ACCULINNA-2 [35] at U-400M heavy ion cyclotron, at Flerov Laboratory of Nuclear Reactions (JINR, Dubna), using the method of double p-^{6}He and triple p-^{6}He-n coincidences, developed in Ref. [36].

A. Experimental setup

The detailed description of the experimental setup is presented in Ref. [4]. Here we provide only a brief account of the major properties of the experimental setup, which we consider useful for the futher discussion. Figure 1 shows schematic layout of the experimental setup with general dimensions.

The 29 A MeV ^{6}He secondary beam was produced with ACCULINNA-2 fragment separator by fragmentation of a primary 33.4 A MeV ^{11}B beam on beryllium target. The standard ACCULINNA-2 scintillator time-of-flight (ToF) stations were used for ^{6}He beam energy measurements for each event. The multiwire proportional chambers MWPC-1 and MWPC-2 provided secondary beam track reconstruction. A cryogenic cell filled with deuterium gas D_2 with a thickness of $3.4(5) \times 10^{20}$ atom/cm^2 was used as a physical target. The protons from the reaction were registered by four telescopes (p telescopes), each consisting of two layers of double-sided silicon

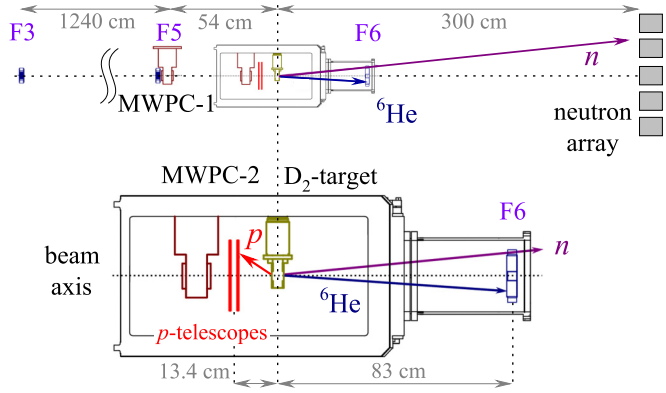

FIG. 1. Layout of the experimental setup. The ToF scintillator detectors are located at F3, F5, and F6; MWPC-1 and MWPC-2: beam tracking detectors. Arrows show typical tracks of the ^{2}H(^{6}He, ^{1}H) ^{7}He reaction products.

strip detectors. The telescopes covered the $\approx 150^\circ$–170° range of laboratory angles.

The ToF base F5–F6 was used for measurement of the heavy reaction fragment (^{4,6}He) longitudinal velocity. Also the energy deposit in thin plastic at F6 was used for the heavy particle identification. The two-dimensional time-amplitude spectrum of the F6 ToF-detector is shown in Fig. 2. The resolution makes it possible to identify only Z of the heavy fragment. However, this is sufficient to significantly suppress the background level in ^{7}He missing mass (MM) spectrum obtained in coincidence with the F6 detector.

The array of the 48 neutron detectors [37] was used for registration of neutrons originating from the ^{7}He decay. Detection of a neutron from the ^{7}He decay allows complete kinematics reconstruction for the ^{2}H(^{6}He, ^{1}H) ^{7}He reaction. This gives additional opportunities for ^{7}He structure studies discussed in the Secs. II B and II C.

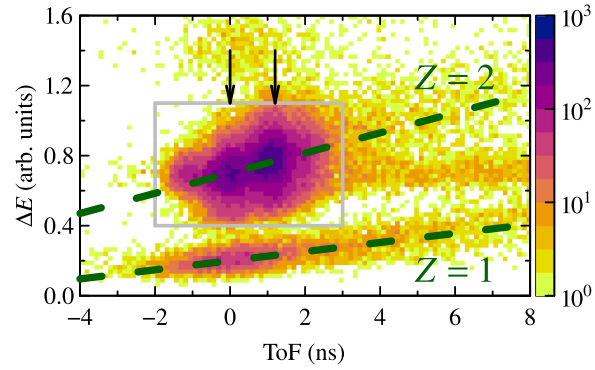

FIG. 2. The ΔE-ToF ID plot for the F5–F6 ToF detectors. Dashed lines mark location of $Z = 1$ and $Z = 2$ heavy fragments. Arrows mark the locations of events connected with unreacted beam (left arrow, ToF $\equiv 0$) and ^{7}He g.s. (right arrow). The gray rectangle indicates the data selection used in the analysis, see Fig. 3.

B. Combined mass

Important opportunity connected with neutron data is the complete-kinematics reconstruction of events. The registration of neutrons from the ^{7}He decay provides information about its decay properties, in particular, the decay energy. The neutron-coincidence events formally contain redundant information about ^{7}He decay energy and there exists an approach that allows to use this redundant information for improvement of the experimental resolution.

The following procedure is used. The velocity of the ^{7}He center of mass is deduced from the momenta of the beam particle and the recoil proton. Using this velocity the momentum of neutron in the ^{7}He center-of-mass system (c.m.s.) can be calculated. For the case of two-body decay, the neutron momentum is sufficient for the ^{7}He decay energy reconstruction. This method of the decay energy reconstruction can be called combined mass (CM) method, see Ref. [38] for another application of such an approach. As far as the measurements of the neutrons' momenta are relatively precise and neutrons carry away the most of the decay energy, the combined mass spectrum reconstruction appears to be drastically more precise compared to the MM method. The Monte Carlo simulations of the experimental setup show that the energy resolution of the CM method is about four times better than the MM energy resolution at energies around the ^{7}He ground state.

C. Correlation measurements

There are two important opportunities connected with registration of the p-n-He coincidences: (i) selection of events in the kinematical locus of the reaction can drastically reduce the background level; (ii) due to the direct mechanism of the ^{2}H(^{6}He, ^{1}H)^{7}He reaction the ^{7}He decay products momenta have specific correlations, which are sensitive to the ^{7}He structure.

As it is shown in Sec. IV, in the frame of PWBA model the reaction ^{2}H(^{6}He, ^{1}H)^{7}He has two transferred momenta: $\mathbf{q}_1$ (momentum transferred to spectator—final-state proton momentum in the deuteron rest frame) and $\mathbf{q}_2$ (momentum transferred to participant-target ^{7}He system—deuteron momentum in the ^{7}He center-of-mass frame). Within the PWBA model the $\mathbf{q}_2$ vector provides the alignment direction around which the ^{7}He decay products should be strongly correlated.

Ordinarily the center of mass angular distributions are used to deduce spin-parities of the states populated in the direct reactions, see Refs. [2,3] for the ^{7}He studied previously in the (d, p) reaction. However, in addition to that, the correlations in the decay of particle-unstable ^{7}He can be studied to deduce this information, see examples of such studies of ^{5}H, ^{9}He, and ^{10}He systems in Refs. [29,39–42]. For the events with neutron coincidences (with complete kinematics) the corresponding correlation functions can be directly extracted from data. This analysis is discussed in the Sec. VII B.

Because the experimental setup accepts only the events where the alignment direction is approximately opposite to the beam direction, this effect should show itself in the distribution of the heavy reaction fragment over the longitudinal velocity. Analysis of this data is discussed in the Sec. VII A.

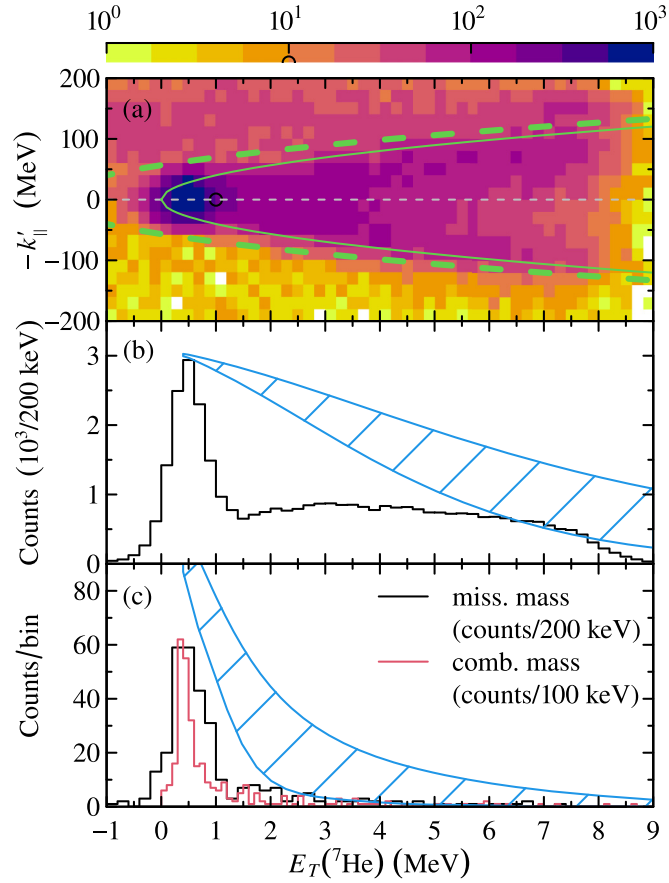

FIG. 3. (a) The heavy decay fragment longitudinal momentum in the ^{7}He center-of-mass system vs ^{7}He missing mass. The solid curve shows the kinematical locus of the ^{2}H(^{6}He, ^{1}H)^{7}He reaction. Dashed curve shows the kinematical cut used in the analysis according to the experimental resolution. (b) The ^{7}He MM spectrum. The hatched region shows the efficiency behavior according to MC simulations: the lower boundary was obtained assuming uncorrelated emission of ^{7}He, and the upper boundary was obtained assuming maximum correlated parabolic (concave) distribution in the $Z||\mathbf{q}_2$ frame. (c) The ^{7}He MM spectrum obtained in coincidence with neutrons and ^{7}He combined mass spectrum. The hatched region shows efficiency behavior evaluated in the same way as in (b).

III. HELIUM-7 EXCITATION SPECTRUM

With the experimental setup Fig. 1 a standard way to get the ^{7}He spectrum is construction of its missing mass by using the information from the detection of a proton recoil. Figure 3(a) shows the ^{7}He MM augmented with information from the forward ToF detector—registration of ^{6}He and ^{4}He heavy products from the ^{7}He decay, see the gray rectangle in Fig. 2. The ToF data here is recalculated in terms of the heavy fragment longitudinal momentum $k'_{\|}$ in the ^{7}He frame. It can be seen in this plot that the MM background conditions are quite good in the experiment, with the major background contribution coming from the random coincidences with the ^{6}He beam located at about $k'_{\|} \approx 130$–150 MeV. The kinematical cutoff in this plot allows to drastically reduce the background in the MM ^{7}He spectrum, see the result in Fig. 3(b). It should

be understood that ^{4}He heavy products originating from the $^7\text{He} \rightarrow {}^6\text{He}^* + n \rightarrow {}^4\text{He} + 3n$ decay channel are confined inside the kinematical locus shown in Fig. 3(a), and, thus the MM spectrum of Fig. 3(b) includes this channel as well.

The energy resolution of the ^{7}He MM spectrum in Fig. 3(b) was obtained as ≈600 keV FWHM in the energy range $0 < E_T < 2$ MeV and 700 keV FWHM in the energy range $6 < E_T < 8$ MeV by the Monte Carlo simulations. The results of the simulations are well confirmed by the observed width of the ^{7}He ground state peak. The ^{7}He MM spectrum has a sharp cutoff at about $E_T \approx 8$ MeV connected with threshold for registration of the slow protons in the backward telescopes. The results of the setup efficiency simulations are shown in Fig. 3(b) by the blue hatched regions. The simulations are shown with arbitrary scaling and normalazed on peak values at 0.4 MeV. The lower bounds of these regions correspond to assumption of isotropic $^7\text{He} \rightarrow {}^6\text{He}^* + n$ decay. The upper bounds correspond to the most extreme correlated decay case when the products are strongly focused in the forward/backward direction in the frame aligned with transferred momentum, see this discussion further in Sec. VII B. This strong focusing is described by pure x^2 term in Eq. (25). Using the efficiency corrections we can find that from 60–75 % of the total cross section with $E_T \lesssim 6$ MeV are connected with population of excited states. In the first instance this may be seen as evidence for low spectroscopy of the ^{6}He g.s. configuration in ^{7}He g.s. structure.

A more advanced treatment of the ^{7}He is available using the information from neutron coincidence data. It can be seen in Fig. 3(c) that efficiency of the neutron wall is something around 3% on the ^{7}He g.s. and it rapidly drops down at $E_T > 1$ MeV rendering the spectrum practically nonexistent at $E_T \approx 2$–3 MeV. As it was discussed above in Sec. II C the combined mass spectrum reconstruction appears to be drastically more precise compared to missing mass providing the ≈150 keV FWHM energy resolution for the ^{7}He g.s., see the red histogram in Fig. 3(c).

The precise measurement of the ^{7}He g.s. width may furnish additional information about ^{7}He structure. The widely used nuclear levels compilation [43] provides $\Gamma = 0.15(2)$ MeV for the ^{7}He g.s. In the further works [6,22,44–46] the estimates of Γ are provided in the range 0.12–0.19 MeV. It should be noted that none of these works have made a crucial effort to determine this value precisely and disagreement among different experimental values is typically larger than their declared errors. The combined mass method gives a high enough resolution for the ^{7}He g.s. width estimation. Such kind of estimates have been given in Ref. [4]. In this paper we present the results of more enhanced analysis of the ^{7}He g.s. parameters. The ^{7}He combined mass spectrum is shown in Fig. 4 on a larger scale together with MC simulations for different ^{7}He g.s. widths values. The analysis of the χ^2 analysis, see the inset in Fig. 4, gives estimates of the resonance energy $E_r = 0.41(2)$ and width $\Gamma = 0.14(5)$ MeV. The errors (confidence intervals) we define by a criterion $\chi^2/N_{\text{df}} = 1$. One can see that the new results is quite close to the results of [4] ($E_r = 0.38(2)$ and $\Gamma = 0.11(3)$ MeV). However, the new Γ estimate have greater value and it

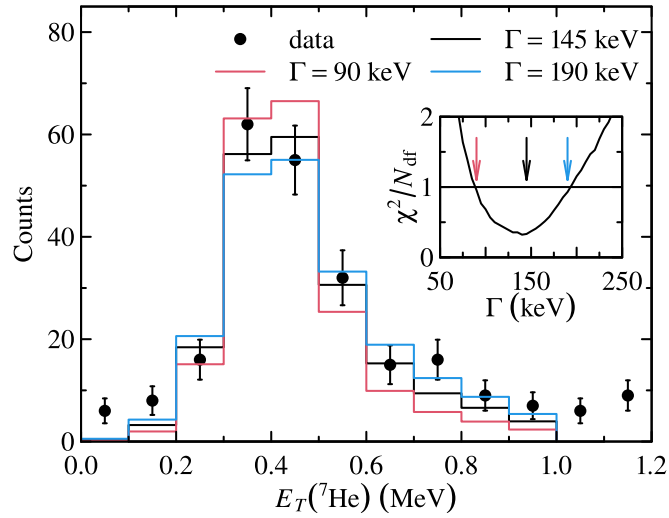

FIG. 4. Results of the MC simulations of the ^{7}He g.s. combined mass spectrum for different assumed widths (histograms) in comparation with the experimental spectrum (circles). The insert shows χ^2/N_{df} criteria as function of the ^{7}He g.s. width. The arrows in the insert correspond to the width values of the presented histograms.

confidence interval is significantly wider, therefore it is consistent with the results of the majority of previous works. We consider that obtained precision for Γ value is mainly determined not by measurement method, but by the available statistics. According to our estimates, in a prospective experiment in analogous technique (with reasonable statistics) the precision $\Delta\Gamma \approx 10$–15 keV could be achieved.

IV. PWBA MODEL FOR THE ^{2}H(^{6}He, ^{1}H)^{7}He REACTION

Important qualitative features of the ^{2}H(^{6}He, ^{1}H)^{7}He reaction can be understood based on the plane-wave Born approximation (PWBA) model, which well reflects the quasifree scattering aspect of the process. For historical reason for this class of reactions we use the notation of the antilab system, where the ^{6}He is considered as target M_t, and the ^{2}H—as composite beam particle M_b, consisting of spectator M_s (proton) and participant M_p (neutron), see Fig. 5. The experiment considered in this work is performed in the inverse kinemat-

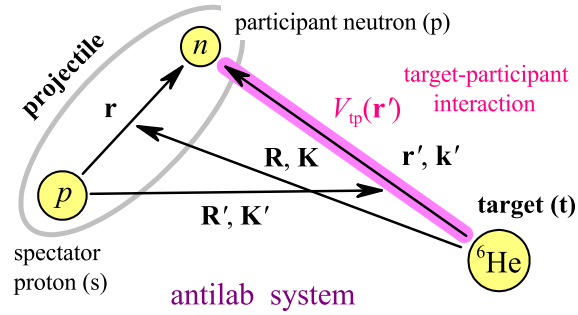

FIG. 5. Prior and post Jacobi coordinate settings for the PWBA model in the (historically motivated) antilab system. Only one final state interaction is taken into account in T-matrix in this approximation.

ics and it should be kept in mind that the beam and target notations are reversed for theoretical discussion of this section. Completely analytical treatment of the model is possible under two essential physical assumptions: plane-wave motion is assumed in the initial $\{\mathbf{R}, \mathbf{K}\}$ and final-state coordinates $\{\mathbf{R}', \mathbf{K}'\}$; and only one interaction is taken into account in the T matrix—the potential $V_{\rm tp}$ between target and participant fragment.

There is some confusion in terminology, but it looks that the most widespread reading is that quasifree scattering (QFS) is further simplification of PWBA, when the off-shell T matrix is replaced with the experimental or phenomenological cross section (on-shell T matrix), sometimes with simple extrapolation in the off-shell region.

Since the 1950s [47,48] this approach was elaborated on numerous occasions ([49] and Refs. therein). It was especially popular for reactions with nucleon transfer from deuteron, having the low binding energy and huge geometric extent, which make the above physical approximations easy to justify. Nevertheless, we found it necessary to provide a detailed discussion of the model in this work for several reasons: (i) it is difficult to find in the literature consistent discussion of the method in the aspect concerning correlations in the decay of unstable product; (ii) the approach has never been discussed in sufficient details in our previous experimental works [29,39–42]; (iii) the rather detailed discussion of correlations in this work would be hard to follow otherwise.

Figure 5 shows the Jacobi coordinates for prior and post forms of the wave function. These sets have a simple relations

$$\mathbf{r}' = \mathbf{R} + \alpha\mathbf{r}\ , \quad \alpha = \frac{M_s}{M_s + M_p}, \quad \beta = \frac{M_t}{M_t + M_p}\ ,$$
$$\mathbf{R}' = -\beta\mathbf{R} + \gamma\mathbf{r}\ , \quad \gamma = \frac{M_p(M_t + M_p + M_s)}{(M_s + M_p)(M_t + M_p)}.$$

The corresponding Jacoby momenta in this notation have the following meaning: $\mathbf{K}$ is the beam momentum in the reaction c.m.s. (the deuteron momentum for the case of the current experiment); $\mathbf{K}'$—momentum of the target-participant subsystem in the reaction c.m.s. (^{7}He momentum); $\mathbf{k}'$—momentum of the participant (neutron) in the target-participant subsystem c.m.s. With the plane-wave in and out WFs

$$\Psi_{tb} = \chi_{\mu_b} e^{i\mathbf{K}\mathbf{R}}, \quad \Psi_{s(tp)} = \chi_{\mu_s} e^{i\mathbf{K}'\mathbf{R}'},$$

the T matrix has explicitly factorized form (the ^{6}He target particle is spinless)

$$T_{\mu'_p,\mu'_s,\mu_b}(\mathbf{K}', \mathbf{k}', \mathbf{K}) = \int d^3r\, d^3R\ \Psi^\dagger_{tp}(\mathbf{k}', \mathbf{r}')\Psi^\dagger_{s(tp)}(\mathbf{K}', \mathbf{R}') \times V_{tp}(\mathbf{r}')\Psi_{sp}(\mathbf{r})\,\Psi_{tb}(\mathbf{K}, \mathbf{R}) = \sum_{\mu_p} T^\dagger_{\mu'_p,\mu_p}(\mathbf{k}', \mathbf{q}_2)\ \Phi_{\mu'_s,\mu_p,\mu_b}(\mathbf{q}_1), \quad (1)$$

where the initial state effects are realized via formfactor Φ, while the target-participant interaction properties are reflected in the off-shell T matrix $T(\mathbf{k}', \mathbf{q}_2)$ of the quasifree subsystem.

It should be emphasized that there are two transferred momenta in the model: $\mathbf{q}_1$ (momentum transfer to spectator in the projectile rest frame) and $\mathbf{q}_2$ (momentum transfer to the quasifree channel). These momenta are defined by relation between initial and final state Jacobi coordinates:

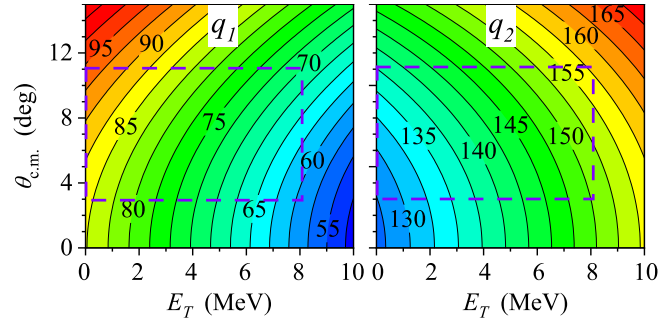

FIG. 6. The transferred momenta $\mathbf{q}_1$ and $\mathbf{q}_2$ as a function of E_T and center of mass reaction angle $\theta_{\rm c.m.}$. The violet rectangles show the kinematical range accessible in the experiment.

$$\mathbf{q}_1 = \alpha\mathbf{K} + \mathbf{K}' \quad , \quad \mathbf{q}_2 = \mathbf{K} + \beta\mathbf{K}'. \quad (2)$$

The behavior of the transferred momenta within the kinematical range of interest for the experimental conditions is illustrated in Fig. 6.

The transfer formfactor (the simple s-wave deuteron WF Ψ_{sp} is assumed) and the elastic scattering T matrix are defined in a standard way

$$\Phi_{\mu'_s,\mu_p,\mu_b}(\mathbf{q}) = C^{1\mu_b}_{1/2\mu'_s 1/2\mu_p} \int d^3r\ \chi^\dagger_{\mu'_s}\chi^\dagger_{\mu_p} e^{-i\mathbf{q}\mathbf{r}}\ \Psi_{sp}(\mathbf{r}),$$
$$T_{\mu'_p,\mu_p}(\mathbf{k}', \mathbf{k}) = \int d^3r\ \chi^\dagger_{\mu'_p} e^{-i\mathbf{k}'\mathbf{r}}\, V_{tp}(\mathbf{r})\,\psi_{tp}(\mathbf{k}, \mathbf{r})\ . \quad (3)$$

The triple-differential cross section is

$$\frac{d\sigma}{dE_T\, d\Omega_{K'}} = \frac{M_{bt}\, M_{s(tp)}}{(2\pi)^2}\ \frac{K'}{K}\ \frac{2M_{tp}k'}{\pi} \times \left[(4\pi)^2\ |\phi_0(q_1)|^2 \sum_{jl} \frac{2j+1}{2s_p+1}\ |T_{jl}(q_2, k')|^2\right], \quad (4)$$

and fivefold-differential cross section suitable for ^{7}He correlation studies can be presented in the density-matrix formulation, which is specially convenient for the further phenomenological studies

$$\frac{d\sigma}{dE_T\, d\Omega_{K'}\, d\Omega_{k'}} = \frac{M_{bt} M_{s(tp)}}{(2\pi)^2}\ \frac{K'}{K}\ \frac{2M_{tp}k'}{\pi} \times \sum_{j'l'm'_j} \sum_{jlm_j} \rho^{j'l'm'_j}_{jlm_j} \sum_{\mu'_p} A^\dagger_{j'l'm'_j\mu'_p}\ A_{jlm_j\mu'_p}. \quad (5)$$

The density matrix depends on the excitation energy

$$E_T = \frac{k'^2}{2M_{tp}}\ ,$$

and the center-of-mass reaction angle $\theta_{\rm c.m.}$, associated with the momentum $\mathbf{K}'$, while the transition amplitudes depend on

$\theta_{\rm c.m.}$ and $\mathbf{k}'$

$$\rho(E_T,\theta_{\rm c.m.})^{j'l'm'_j}_{jlm_j} = (4\pi)^2\,|\phi_0(q_1)|^2\,M^{j'l'm'_j}_{jlm_j},$$

$$A_{jlm_j\mu'_p}(\theta_{\rm c.m.},\mathbf{k}') = \frac{\hat{j}}{\hat{s}_p}\,T_{jl}(q_2,k')\sum_m C^{jm_j}_{lms_p\mu'_p}\,Y_{lm}(\hat{k}'). \quad (6)$$

The partial components of the elastic T matrix and transfer formfactor for the simple s-wave deuteron WF with radial component $\psi_0(r)$ are defined as

$$T_{jl}(k',k) = \frac{1}{k'k}\int dr\,F_l(k'r)\,V_{tp}(r)\,\psi_{jl}(kr), \quad (7)$$

$$\phi_0(q) = \frac{1}{q}\int dr\,F_0(qr)\,\psi_0(r). \quad (8)$$

The matrix M is pure angular density matrix

$$M^{j'l'm'_j}_{jlm_j} = \frac{4\pi}{\hat{j}'\hat{j}}\sum_{m'm\mu_p} C^{j'm'_j}_{l'm's_p\mu_p}C^{jm_j}_{lms_p\mu_p}Y^*_{l'm'}(\hat{q}_2)Y_{lm}(\hat{q}_2), \quad (9)$$

with symmetries

$$\langle j'l'm|\rho|jlm\rangle = (-)^{l+l'-j-j'+1}\,\langle j'l'-m|\rho|jl-m\rangle, \quad (10)$$

It is normalized to give unity for each $\{j,l\}$ state

$$\textstyle\sum_{m_j} M^{jlm_j}_{jlm_j} \equiv 1.$$

The maximum spin alignment in the quasifree ^{7}He channel is realized in the system, where $Z||\mathbf{q}_2$. In this frame the density matrix gets the most sparse and simple form. For the $\{s_{1/2}, p_{1/2}, p_{3/2}\}$ state vector one gets

$$M^{j'l'm'_j}_{jlm_j} = \begin{pmatrix} 1/2 & 0 & -1/2 & 0 & 0 & 1/2 & 0 & 0\\ 0 & 1/2 & 0 & 1/2 & 0 & 0 & 1/2 & 0\\ -1/2 & 0 & 1/2 & 0 & 0 & -1/2 & 0 & 0\\ 0 & 1/2 & 0 & 1/2 & 0 & 0 & 1/2 & 0\\ 0 & 0 & 0 & 0 & 0 & 0 & 0 & 0\\ 1/2 & 0 & -1/2 & 0 & 0 & 1/2 & 0 & 0\\ 0 & 1/2 & 0 & 1/2 & 0 & 0 & 1/2 & 0\\ 0 & 0 & 0 & 0 & 0 & 0 & 0 & 0 \end{pmatrix}.$$

The scattering WF $\psi_{jl}(kr)$ diagonalizing the elastic S matrix, is normalized by the asymptotic condition

$$\psi_{jl}(kr) \to e^{i\delta_{jl}}\,\sin(kr - l\pi/2 + \delta_{jl}).$$

For that reason the PWBA transition amplitude can be represented as

$$\frac{\hat{j}}{\hat{s}_p}\,T_{jl}(q_2,k') = a_{jl}(q_2,k')\,e^{i\delta_{jl}(E_T)}, \quad (11)$$

where the a_{jl} are real-valued functions. For reactions well suited for the quasifree approximation, we may expect, although can not be completely confident, that the real transition amplitudes and phases are reasonably close to the PWBA values. The population probabilities for different states can be defined as

$$W_{jl}(q_2,k') = S_{jl}\,\frac{2M_{tp}k'}{\pi}\,a^2_{jl}(q_2,k'), \quad (12)$$

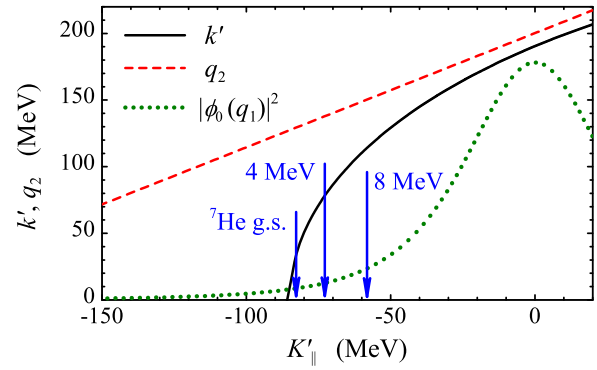

FIG. 7. The values of $\mathbf{k}'$ and $\mathbf{q}_2$ as a function of laboratory momentum of the recoil proton $K'_\parallel$ at $K'_\perp \equiv 0$, which also corresponds to the reaction laboratory angle $\theta_{\rm c.m.} = 0$ and relation $q_1 = K'_\parallel$. The ^{7}He threshold energies $E_T = \{0.45, 4, 8\}$ MeV are indicated by the vertical blue arrows. The deuteron form factor $|\phi_0(q_1)|^2$ (green dotted curve) is shown with arbitrary scaling.

where phenomenological corrections, if necessary, are included via spectroscopic factors S_{jl}.

The correlations pattern for the $\{s_{1/2}, p_{1/2}, p_{3/2}\}$ state set in the frame where $\mathbf{q}_2$ directed along Z axis can be obtained as (case of a complete equatorial alignment)

$$\frac{d\sigma}{dx} \propto \frac{1}{2}a^2_{s_{1/2}} + \frac{1}{2}a^2_{p_{1/2}} + \frac{1}{4}a^2_{p_{3/2}}(1+3x^2) + \frac{1}{\sqrt{2}}a_{p_{1/2}}a_{p_{3/2}}(3x^2-1)\cos\left(\delta^{p_{3/2}}_{p_{1/2}}\right) + a_{s_{1/2}}x\left[a_{p_{1/2}}\cos\left(\delta^{p_{1/2}}_{s_{1/2}}\right) + \sqrt{2}a_{p_{3/2}}\cos\left(\delta^{p_{3/2}}_{s_{1/2}}\right)\right], \quad (13)$$

where the x variable and the relative phases are

$$x = \cos(\theta_{k'}) \equiv \cos(\widehat{\mathbf{k}',\mathbf{q}_2}), \quad \delta^{j_1l_1}_{j_2l_2} = \delta_{j_1l_1} - \delta_{j_2l_2}. \quad (14)$$

There are two important features clarified within the PWBA model at that point:

(i) The (d,p) reaction for our kinematical conditions are not comfortable for interpretation in terms of quasifree scattering. The values of $\mathbf{k}'$ and transferred momentum $\mathbf{q}_2$ entering the $T(q_2,k')$ are shown in Fig. 7. The off-shell effect is large in this reaction and this effect is strongly varying across the ^{7}He excitation energy range $E_T \lesssim 8$ MeV accessible in the experiment. According to Fig. 7 one may expect that quasifree scattering approximation may become safe (small off-shell corrections) at $E_T \approx 20$–30 MeV.

(ii) In the energy range of interest, the deuteron form factor $|\phi_0(q_1)|^2$ value vary by factor 2–3. Thus, the population of the ^{7}He excitation spectrum does not provide the direct information on spectroscopy of ^{7}He excited states: within PWBA model this information for broad excited state of ^{7}He is expected to be strongly effected by the reaction mechanism.

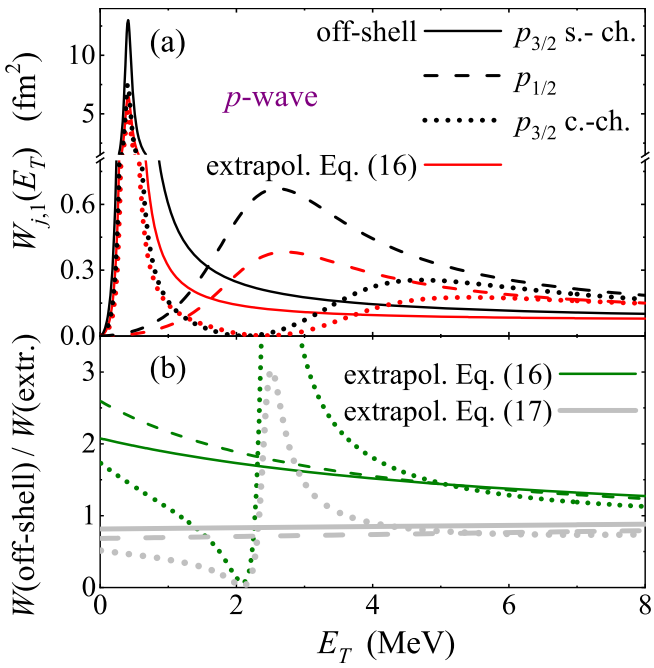

FIG. 8. (a) The $l = 1$ population probabilities Eq. (12) calculated off shell at $\theta_{\rm c.m.} = 8^\circ$, where most of the data are located, and extrapolated from the on-shell value by Eq. (16). (b) Ratios of the directly calculated off-shell probabilities to the two variants of the extrapolated from the on-shell values, by Eq. (16) and by Eq. (17). Calculations in the single-channel potential model for the $p_{3/2}$ and $p_{1/2}$ resonances and the coupled-channel model for the $p_{3/2}$ resonance are shown in the panels by solid, dashed and dotted lines, respectively.

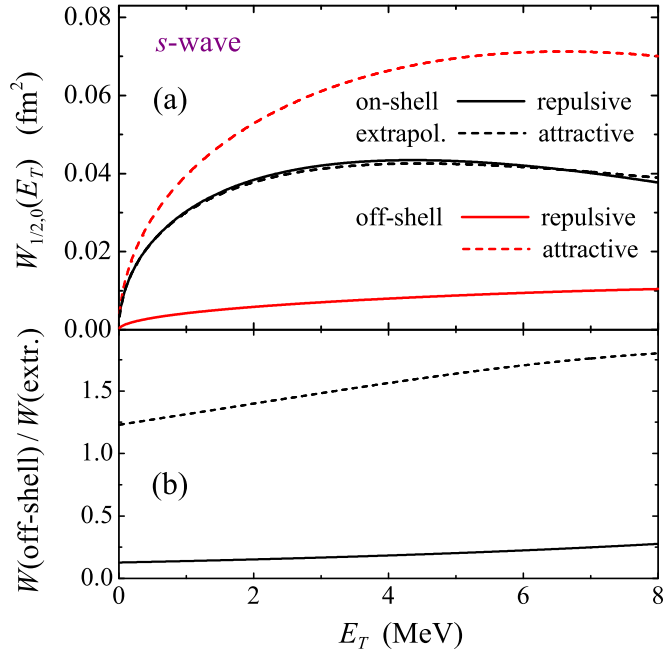

FIG. 9. (a) The s-wave population probabilities Eq. (12) calculated off shell at $\theta_{\rm c.m.} = 8^\circ$, and extrapolated from the on-shell value by Eq. (16). (b) Ratios of the directly calculated off-shell probabilities to the extrapolated on-shell values.

V. MODELS FOR THE ^{7}He CONTINUUM

The easiest approximation for the ^{7}He continuum states are provided by the single-channel potential model. For simplicity we used the square-well nuclear potential, which is sufficient for qualitative considerations and allows to make most of calculations analytically.

A. $p_{3/2}$ ground state

The ^{7}He ground state width is around 140 keV. With potential of reasonable radius $r_0 = 3$ fm one get width of ≈250 keV. To play with the width values in potential model we can vary the potential width. This is not quite consistent with physics of the case, where reduction on the ^{7}He g.s. is connected with not single-particle nature of this state [strong mixing with ^{6}He$(2^+) + n$ configuration]. The $p_{3/2}$ continuum profile calculated with $r_0 = 1.86$ fm and giving $\Gamma = 140$ keV are shown in Fig. 8(a). In this model the high-energy potential tail of the $p_{3/2}$ resonance is scaled as r_0. This behavior is important for understanding of the $p_{1/2}$ state properties (discussed below) and correlations (see Sec. VII A 2).

Within the QFS approximation to PWBA [4,5] instead of the off-shell T matrix the phenomenological on-shell cross section is used, which is extrapolated off-shell in some reasonable way. The on-shell population probability Eq. (12) is related to the elastic cross section $\sigma^{(\rm el)}$ as

$$W_{jl}(k', k') = \frac{\sin^2 \delta_{jl}}{2\pi M_{tp} k'} = \frac{k' \sigma^{(\rm el)}_{jl}(E_T)}{8\pi^2 M_{tp}}. \qquad (15)$$

From the T-matrix definition (7) a reasonable off-shell extrapolation is

$$W_{jl}(q_2 > k', k') = \frac{k' P_l(q_2)}{q_2 P_l(k')} W_{jl}(k', k') \qquad (16)$$

$$\approx \left(\frac{q_2}{k'}\right)^{2l} W_{jl}(k', k'), \qquad (17)$$

see, e.g., Refs. [49,50]. It is evidently precise in the low q_2 limit, which is not a good approximation for the experimental conditions, see Fig. 7. Nevertheless, it can be found in Fig. 8(b) that the off-shell extrapolation (17) is quite precise in the case of p-wave states, represented by potential scattering. In the coupled-channel case the extrapolations work poorly in a broad energy range including the g.s. energy region.

B. $s_{1/2}$ state

It is typically expected that interaction in this partial wave is quite featureless repulsion. The $s_{1/2}$ continuum profiles calculated with repulsive potential and deep attractive potential (with forbidden state) are shown in Fig. 9. The phase shifts for these cases are fine tuned to be very close to each other and to the phase shifts obtained in sophisticated continuum shell-model calculations [24,34]. One may see in Fig. 9 that the off-shell T matrices are (i) strongly (factor 5–8) different depending on specific dynamics and (ii) they are evidently not off-shell extrapolatable by simple expressions like Eq. (16).

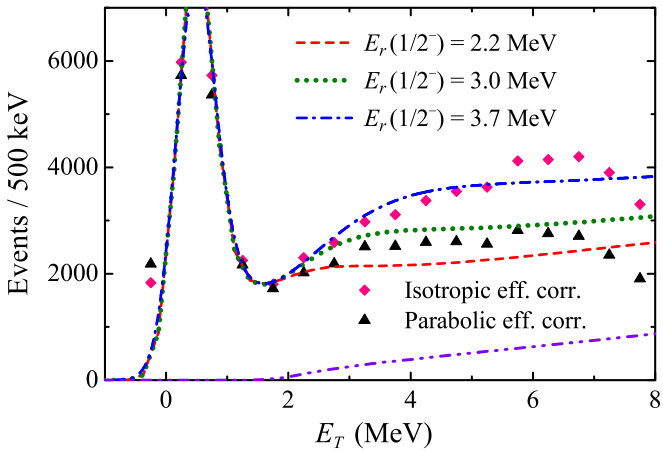

FIG. 10. The ^{7}He state profiles provided by potential model for different positions of the $p_{1/2}$ resonance (attractive s-wave potential) are compared with the data, see also Fig. 15(b). The data are efficiency corrected by MC simulations in two ways: assuming uncorrelated emission of ^{7}He and maximally correlated parabolic (concave) distribution in the $Z||\mathbf{q}_2$ frame (see also Fig. 3). The possible contribution of the decay channels $^7\text{He} \rightarrow {}^6\text{He}^* + n$, connected with disintegration of $^6\text{He} \rightarrow \alpha + n + n$ are extrapolated by using the data from [3].

This is demonstration that treatment of the s-wave populations in reactions should be considered with more caution. This fact is also important for discussion of possible interpretation of correlations in terms of s-wave resonance contributions, see Sec. VII A 3.

For attractive potential the PWBA s-wave population is on the upper limit of what is admissible from experimental data, see the next section. So, phenomenologically this population can not be increased, but can be reduced (e.g., repulsive potential). From correlations point of view if we reduce the s-wave population of Fig. 9 50-fold, it will be still sufficient to provide experimentally observed backward-forward asymmetry, see Sec. VII A.

C. $p_{1/2}$ state

Quite reliable evidence for this state may be found in the data as a dip in the ^{7}He spectrum at $E_T = 1.5$–1.8 MeV and corresponding kink in the spectrum at $E_T \approx 3$ MeV. However, the $1/2^-$ peak is sitting on a strong background of the $3/2^-$ and $1/2^+$ contributions, which are in general case comparable and not completely fixed by theoretical considerations. One of the fits to the data (attractive s-wave potential) is shown in Fig. 10. The spectroscopic factors for the $1/2^-$ state are deduced by requesting a good fit quality in the energy range $E_T \approx 1$–3 MeV are listed in the Table I. The $1/2^-$ is expected to be a single-particle state with spectroscopic factor close to unity. Requesting the spectroscopic factor to be in the range $S_{p_{1/2}} \approx 0.7-1.3$ we get limits on possible $1/2^-$ spectrum properties. The $1/2^-$ resonant energy positions outside the $E_r = 2.2$–3.0 MeV interval are not acceptable. Considering the results of Sec. VII A 2 as preferable explanation for the observed correlations, $E_r \approx 2.6$ MeV seem to be a preferable value.

TABLE I. Spectroscopic factors $S_{p_{1/2}}$ for the $1/2^-$ state of ^{7}He obtained by fitting the experimental MM spectrum. The spectroscopic factor for the $3/2^-$ g.s. is taken as $S_{p_{3/2}} = 0.5$. Abbreviation FC stand for Fermi cut of the $3/2^-$ population probability at $E_T \approx 1.2$–1.4 MeV, see also Sec. VII A 2.

$E_r(1/2^-)$	Attr. $s_{1/2}$	Rep. $s_{1/2}$	Attr. $s_{1/2}$+FC	Rep. $s_{1/2}$+FC
2.2	0.4	0.6	0.9	1.1
2.6	0.6	0.8	1.2	1.4
3.0	0.9	1.2	1.4	1.8
3.7	1.8	2.0	2.8	3.2

D. Coupled-channel $p_{3/2}$ state

Important aspects of the continuum dynamics beyond the single-channel potential approximation can be treated within the coupled-channel formalism. For our purposes we construct the coupled-channel model in a schematic way. The coupled-channel Shrödinger equations look like

$$(\hat{T} - E_T + \hat{V}_{11})\Psi_{He\text{-}n} + \hat{V}_{12}\Psi_{He^*\text{-}n} = 0,$$
$$(\hat{T} - (E_T - \Delta E_T) + \hat{V}_{22})\Psi_{He^*\text{-}n} + \hat{V}_{12}\Psi_{He\text{-}n} = 0\,.$$

The energy E_T is considered from the ^{6}He(g.s.)-n threshold. The ^{6}He(2^+)-n threshold is $\Delta E_T = 1.8$ MeV higher, and it should be understood that this notion is a certain approximation as the ^{6}He(2^+) state is particle unstable. The actual first threshold in the ^{7}He system is the three-body ^{4}He$+3n$ threshold at $E = 0.97$ MeV. The dynamical issue which saves the situation is that below the ^{6}He(2^+)-n threshold the decay mechanism for ^{7}He states is so-called true $3p$ emission, which is strongly suppressed compared to sequential $3p$ emission via the ^{6}He(2^+) state.

The channel potentials $\hat{V}_{ij}$ are obtained from n-n and α-n potentials in the folding model using the realistic ^{6}He WFs, e.g., from Ref. [51]. The SBB α-n interaction [52] is used and simple effective n-n interaction [53]. The diagonal potentials $\hat{V}_{11}$ for the ^{6}He(g.s.)-n channel and $\hat{V}_{22}$ for the ^{6}He(2^+)-n channel are used practically as is (some fine tuning $\lesssim 5\%$ can be applied). In contrast, the off-diagonal potential $\hat{V}_{12}$ typically requires strong modification to provide sufficient coupling to get realistic mixing values for the ^{7}He g.s.; it seem that this aspect of the ^{7}He dynamics is beyond the folding approximation.

An example of the coupled-channel studies is shown in Fig. 8. The population probabilities obtained in this model have the following important features:

(i) The experimental ^{7}He $3/2^-_1$ g.s. width is naturally well reproduced in this model.
(ii) The second $3/2^-_2$ state is found at relatively low energy ($E_T \approx 5.5$ MeV).
(iii) There is a strong dip in the population probability between the $3/2^-_1$ and $3/2^-_2$ states, which could be

important for explanation of correlations in ^{7}He decay, see Sec. VII A 2.

(iv) It can be found in Fig. 8(b) that the off-shell extrapolation, which was quite safe for the single-channel potential model, is not working in the coupled-channel case.

VI. CENTER-OF-MASS ANGULAR DISTRIBUTIONS

The center-of-mass angular distributions provide the standard basis for spin-parity identification in the direct reactions. For the (d, p) reaction in inverse kinematics the recoil protons escaping in the relatively broad (5–30 degrees) angular range in the backward direction in the laboratory system correspond to small c.m.s. angular range (2–11 degrees). Therefore, the use of the (d, p) reaction in our studies has both advantages and disadvantages.

The advantage for interpretation of our result is that population of states with high Δl should be suppressed in this experiment [54]. For example the only state, which is unambiguously identified in the excitation spectrum of ^{7}He is the $5/2^-$ state at $E \approx 3.4$ MeV, which decays with a large ^{6}He(2^+) channel [1,55]. However, population of this state requires $\Delta l = 3$ compared to $\Delta l = 1$ populating the $3/2^-$ and $1/2^-$ states. So, it is quite natural to expect that only the $3/2^-$ and $1/2^-$ resonant states of ^{7}He are strongly populated in this experiment.

The disadvantage of the small angular range is that we are unable to make a detailed comparison of the cross section angular distribution with reaction theory calculations to justify a specific spin-parity prescription. Nevertheless, we are going to demonstrate that important conclusions are possible on the basis of the c.m.s. angular distributions derived in this experiment.

The experimental c.m.s. angular distributions for different excitation energy ranges of ^{7}He are shown in Fig. 11. The data are corrected for the detection efficiency of the setup via the MC procedure. The obtained angular distributions can be considered as independent of energy within the uncertainty of data, that may be a signal, that the same set of weights of different Δl values is valid.

The comparison of experimental data with the PWBA calculations is given in Fig. 12(a). In its basic form, see Sec. IV, the PWBA model is not suitable for calculations of absolute cross sections. However, there is a standard phenomenological modification of the model: the peripheral Fermi-type cutoff for the projectile (deuteron) WF,

$$\psi_0(r) \to \frac{\psi_0(r)}{1 - \exp[(r - r_{\rm cut})/d_{\rm cut}]}.$$

It can be seen in Fig. 12(a) that both the ^{7}He g.s. angular distributions of this work and of Ref. [3] can be reproduced only by different parameter sets. Similary, in the DWBA studies of Ref. [4] somewhat different spectroscopic factor values $S = 0.49$ and $S = 0.39$ were extracted for the 29 A MeV data and for the 11.5 A MeV data of Ref. [3]. Moreover it is demonstrated in Fig. 12(b), that no monotonic function ϕ_0 exists, which can describe both data sets. So, the data sets can not be reconciled within typically used direct reaction

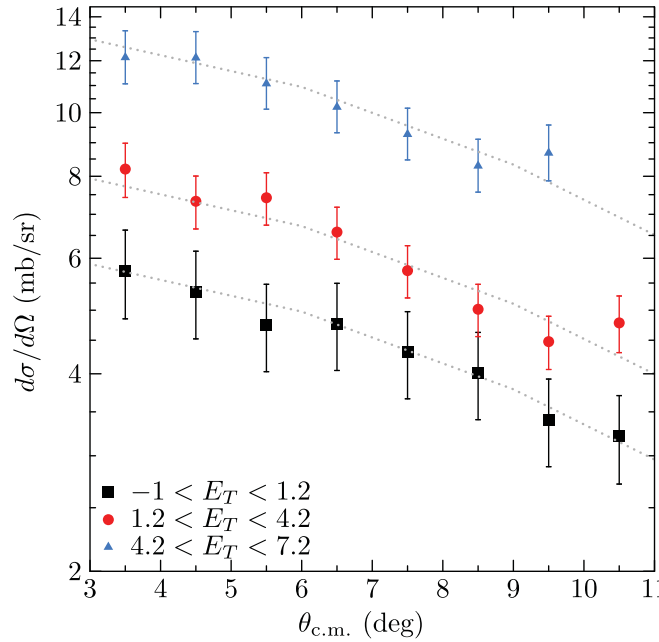

FIG. 11. Differential cross section for the ^{2}H(^{6}He, ^{1}H)^{7}He reaction for different ranges of the ^{7}He decay energy E_T. The dotted lines show the result of PWBA calculation for the ^{7}He $3/2^-$ g.s. (see also Fig. 12) scaled by the factors 1, 1.35, and 2.2 to guide an eye.

theoretical frameworks, and this is a good indication, that absolute calibration of one of the data sets is actually wrong. This situation calls for a more precise experiment.

The stability of the angular distributions, demonstrated in Fig. 11, is quite natural if the obtained data is strongly dominated by the same angular momentum transfer $\Delta l = 1$ ($3/2^-$ g.s., $1/2^-$, and $3/2^-_2$ excited states), in the whole excitation energy range $0 < E_T < 8$ MeV available in the experiment. The observation of the low-lying $s_{1/2}$ resonance in ^{7}He was declared in Ref. [5], which should also exhibit itself in the angular distributions. Unfortunately, it is known, that specifically for the (d, p) reactions the $\Delta l = 0, 1, 2$ cross sections have highly analogous profiles. It can be seen in Fig. 12(c) that to reliably distinguish the $\Delta l = 0$ and $\Delta l = 1$ contributions we should go to $\theta_{\rm c.m.} \gtrsim 20^\circ$ and need a data with a high statistical confidence. It may be possible to prove or disprove the statement about the $s_{1/2}$ resonant state in ^{7}He by performing a dedicated (d, p) experiment, in which a broad c.m.s. angular range is accessible.

VII. CORRELATION STUDIES FOR THE ^{7}He SPECTRUM

It is shown in Sec. IV that the momenta of ^{7}He decay products should be strongly correlated with the $\mathbf{q}_2$ direction. In the experimental statistics there is a subset of events with neutron coincidence and full kinematics. For the events in this subset the value of $\cos\theta_{k'}$ can be extracted from the experimental data and ^{7}He decay energy measured with high resolution ($\lesssim$200 keV FWHM), but this data has a very limited statistics and a strong efficiency cutoff at $E_T \gtrsim 2$ MeV.

In contrast, the longitudinal velocity of the heavy decay fragment (and, correspondingly, the projection of $\mathbf{k}'$ on the

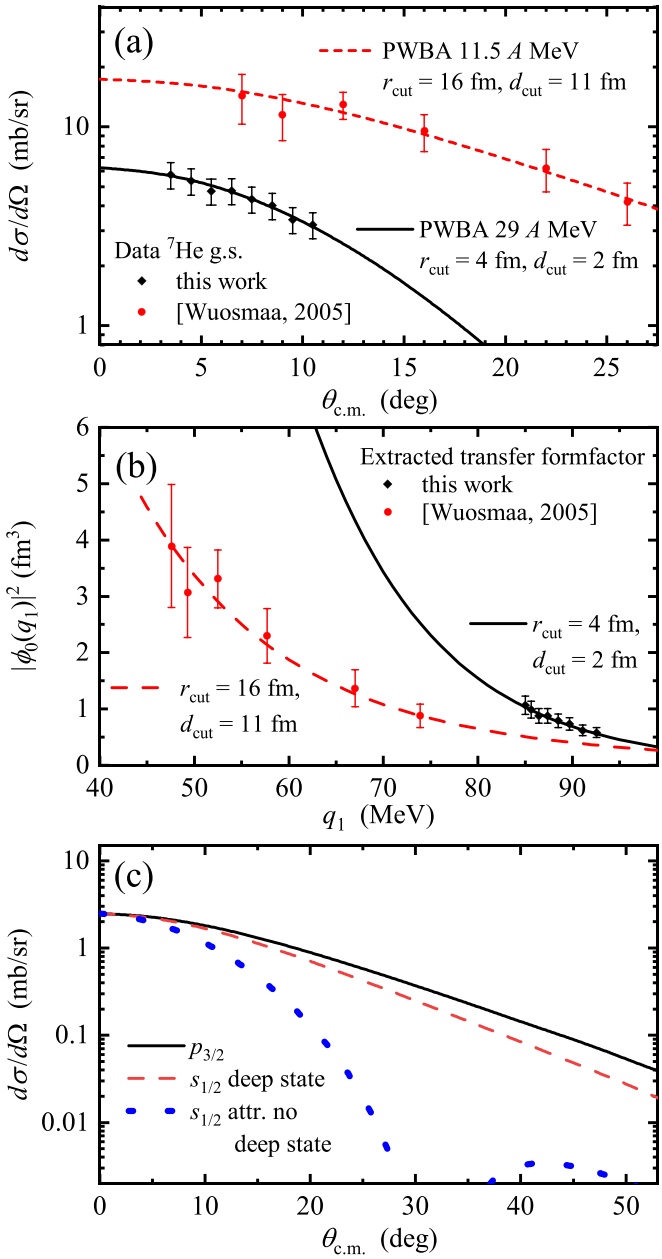

FIG. 12. (a) Comparison of the differential cross sections of the ^{2}H(^{6}He, ^{1}H) ^{7}He reactions populating the ^{7}He g.s. as obtained in this work and work the by Wuosmaa *et al.* [3]. Points show experimental data. (b) Extracted squared transfer formfactor $|\phi_0(q_1)|^2$ from both experimental data are shown by points. The curves correspond to the calculated deuteron formfactor with the corresponding cutoff to show the best fit to the date. (c) PWBA predictions for the angular distributions for $\Delta l = 0$ and $\Delta l = 1$ angular momentum transfers.

beam axis $k'_{\|}$) was measured for all events. For the events accepted by the setup of the experiment the equality

$$\cos(\theta_{k'}) \approx -k'_{\|}/k' \,,$$

is precise within several percent. For this type of the data a broad excitation-energy range $E_T \lesssim 8$ MeV is covered, but also the energy resolution is much lower (≈600 keV FWHM).

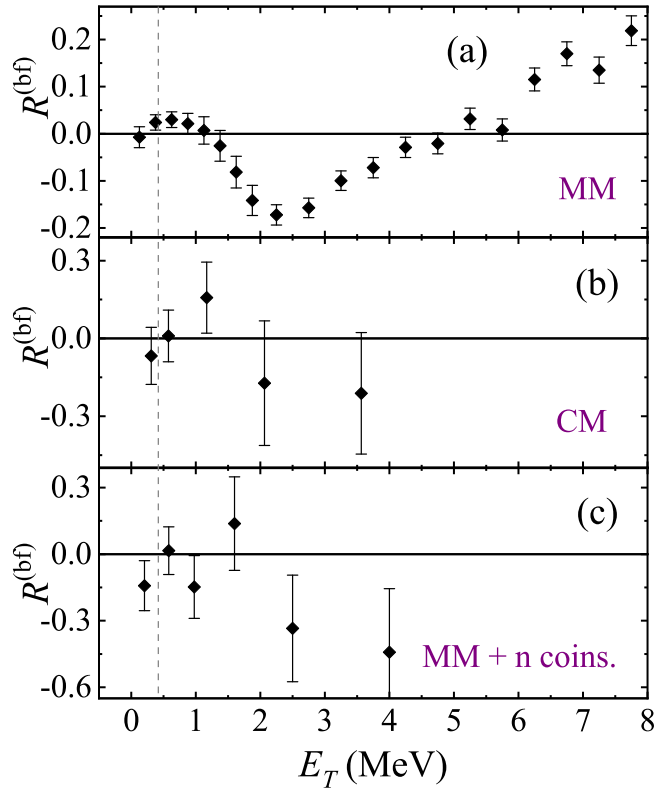

FIG. 13. Experimental backward-forward asymmetry for the ^{7}He decay at different excitation energies for missing mass spectrum (a) and combined mass spectrum (b). The missing mass spectrum with additional neutron coincidence condition (c) is in reasonable agreement with the combined mass spectrum (b) indicating consistent calibrations of these two types of spectra. The vertical dashed line indicates the ^{7}He g.s. position.

Due to low resolution of $k'_{\|}$ and E_T for this data the correlations are available only in the form of backward-forward asymmetry in the ^{7}He frame. Let us first discuss the latter type of the correlations.

A. Backward-forward asymmetry in the distribution of core longitudinal momentum

In our discussion of correlations the forward direction is the direction of $\mathbf{q}_2$ and, correspondingly, $\cos(\theta_{k'}) > 0$ or $k'_{\|} < 0$. The experimental backward-forward asymmetry function is defined as

$$R^{(\mathrm{bf})} = \frac{W_\mathrm{f} - W_\mathrm{b}}{W_\mathrm{f} + W_\mathrm{b}} \,,$$

see Fig. 13. Important feature of this distribution is rise from zero at $E_T \approx 0$ MeV, then quite abrupt change of sign at about $E_T = 1.5$ MeV, and then one more change of sign at $E_T \approx 5$ MeV.

From Eq. (13) the backward-forward asymmetry is obtained as

$$R^{(\mathrm{bf})} = \frac{a_{s_{1/2}}\left[a_{p_{1/2}} \cos\left(\delta^{p_{1/2}}_{s_{1/2}}\right) + \sqrt{2} a_{p_{3/2}} \cos\left(\delta^{p_{3/2}}_{s_{1/2}}\right)\right]}{a^2_{s_{1/2}} + a^2_{p_{1/2}} + a^2_{p_{3/2}}}. \quad (18)$$

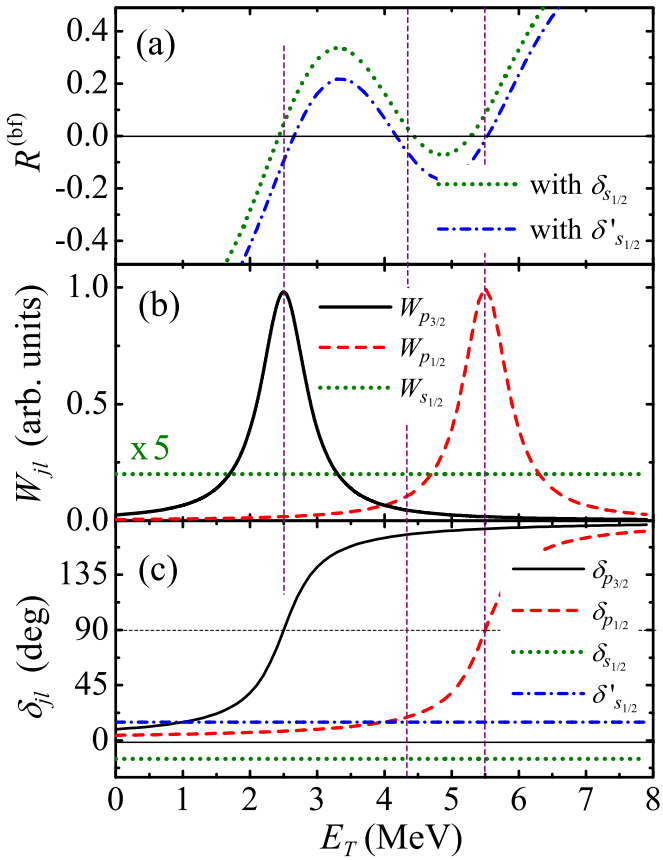

FIG. 14. Asymmetry for the simple model of $\{s_{1/2}, p_{1/2}, p_{3/2}\}$ interference: (a) asymmetry function; (b) population probabilities; (c) phase shifts in the ^{6}He -n channel.

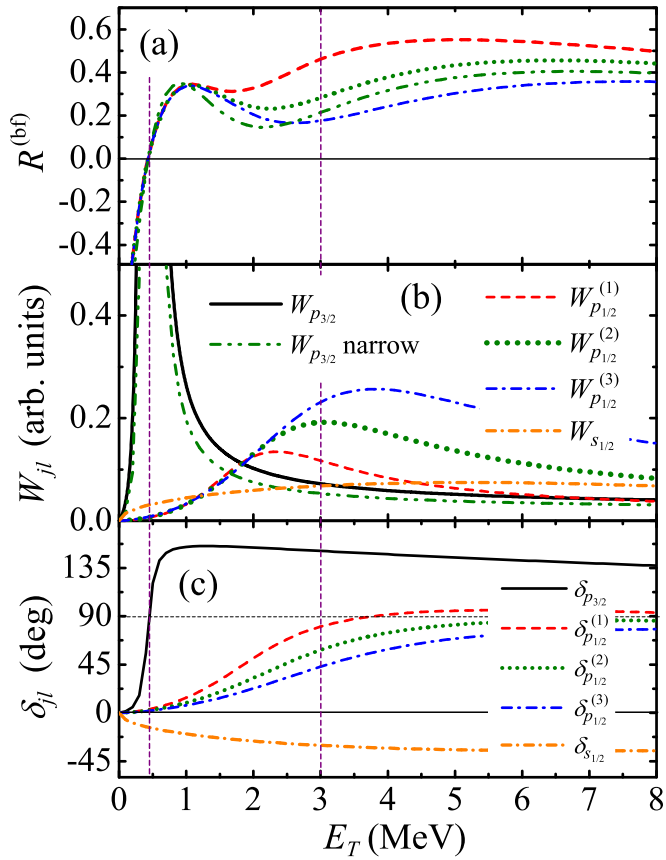

FIG. 15. Asymmetry for $\{s_{1/2}, p_{1/2}, p_{3/2}\}$ interference in PWBA model with single-channel scattering states in the ^{6}He -n channel: (a) asymmetry functions; (b) population probabilities; (c) phase shifts. The maximal variation of the $p_{1/2}$ state position admissible by the data of Fig. 10 is performed.

Let us first demonstrate, how the observed backward-forward asymmetry can be qualitatively explained by a simple example of $\{s_{1/2}, p_{1/2}, p_{3/2}\}$ correlation pattern for narrow p-wave states interference with flat s-wave background, see Fig. 14. The population probabilities (12) and phase shifts for this example are provided by the standard R-matrix parametrization

$$\tan(\delta) = \frac{\Gamma}{2(E_r - E_T)}.$$

We can find that the $R^{(bf)}$ value is changing sign for the first time close to the $p_{3/2}$ resonance position (but not exactly at resonance), at the point where

$$\delta^{p_{3/2}}_{s_{1/2}} \approx \pi/2\,, \tag{19}$$

since the $p_{1/2}$ contribution can be neglected here. The $R^{(bf)}$ value is changing sign for the second time around the point

$$W_{p_{1/2}} \approx 2\,W_{p_{3/2}}\,, \tag{20}$$

where the relative phase shift $\delta_{p_{3/2}} - \delta_{p_{1/2}} \approx \pi$. The third time the sign is changed in analogy with Eq. (19) around the point

$$\delta^{p_{1/2}}_{s_{1/2}} \approx \pi/2\,, \tag{21}$$

where the $p_{3/2}$ contribution can be neglected.

We should also point that even a very small, visually negligible, contribution of the s-wave configuration could be sufficient to produce the typical observed asymmetry rate. The variation of the s-wave phase shift from attraction to repulsion leads only to insignificant variation of the whole correlation pattern, see $\delta_{s_{1/2}}$ and $\delta'_{s_{1/2}}$ cases in Fig. 14.

The use of realistic profiles provided by potential model for the ^{7}He T matrix gives qualitatively similar behavior, but do not provide quantitative agreement, see Fig. 15. There is a kink in the asymmetry function in between the $p_{3/2}$ and $p_{1/2}$ resonances, but the value is not falling towards zero: the effect of the $p_{1/2}$ state seem to be too small and it should be enlarged to achieve agreement with experiment. However, it can be found that contributions of the $p_{1/2}$ resonance are already on the upper limit admissible by the experimental MM spectrum, see Fig. 10. Alternatively we may inquire, whether the contribution of the $p_{3/2}$ state may be reduced at $E_T > 1$–1.5 MeV. It can be seen in Fig. 15 (green double-dotted curve) that within the potential approach even the unrealistically strong variation of the $p_{3/2}$ g.s. properties does not lead to sufficiently strong variation of the high-energy tail of this state. We have found three possible explanations for the data, as listed in the following sections.

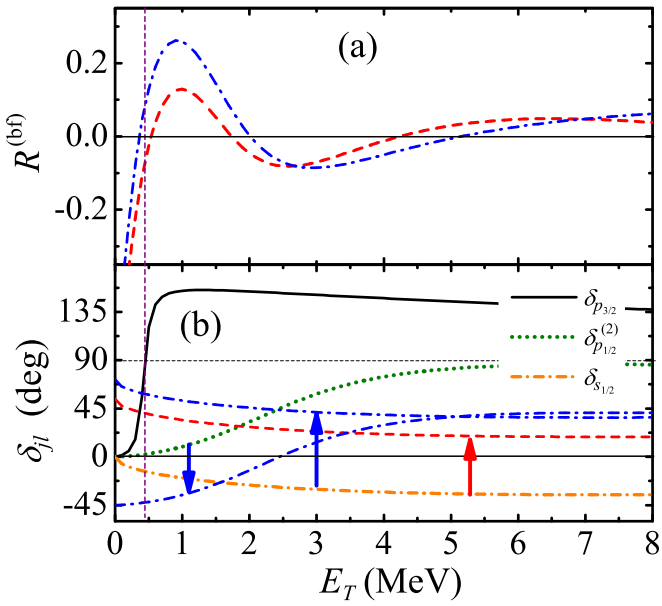

FIG. 16. Asymmetry for $\{s_{1/2}, p_{1/2}, p_{3/2}\}$ interference in PWBA model with modified phase shift convention: (a) asymmetry functions; (b) two variants of of phase shifts modification of Eq. (22) are shown by red and blue curves and correspondingly colored arrows.

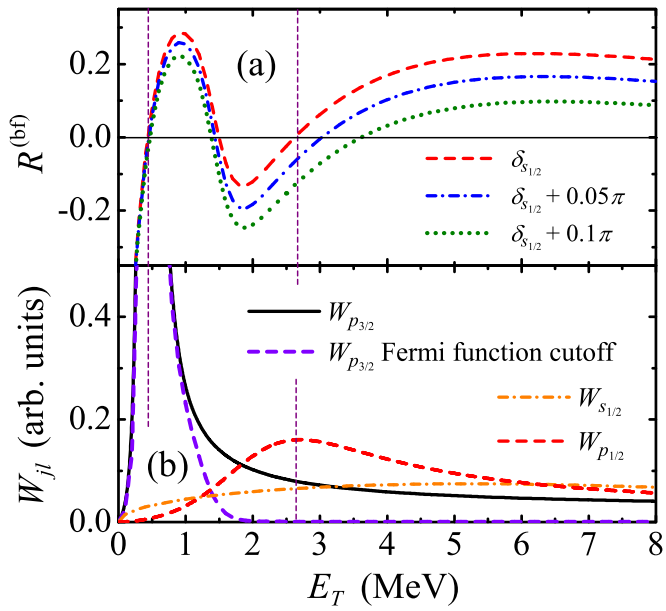

FIG. 17. Asymmetry for $\{s_{1/2}, p_{1/2}, p_{3/2}\}$ interference in PWBA model with single-channel scattering states in the ^{6}He-n channel, but with modified (Fermi function cutoff) high-energy tail of the $p_{3/2}$ resonance: (a) asymmetry function; (b) population probabilities. Small modifications of the $s_{1/2}$ phase shifts may lead to improved agreement with the data.

1. Phase shift variation

The phase behavior of the T-matrix elements is provided in PWBA as elastic phase shift in the ^{7}He channel, see Eq. (11). However, as we have already mentioned in the Sec. IV, that this is not necessarily true in situation with some general reaction mechanism. It can be found that modifications of the T-matrix phase behavior

$$\begin{aligned} \delta_{s_{1/2}} &\to \delta_{s_{1/2}} + 0.3\pi\,, \\ \{\delta_{s_{1/2}}, \delta_{p_{1/2}}\} &\to \{\delta_{s_{1/2}} + 0.4\pi\,,\ \delta_{p_{1/2}} - 0.25\pi\}\,, \end{aligned} \tag{22}$$

lead to results reasonably consistent with experimental observations, see Fig. 16. The first variant of modification in Eq. (22) looks more realistic, since the relative phase shift of s-wave and p-wave T matrices looks quite reasonable, say within DWBA, while the sizable relative phase shift of the $p_{3/2}$ and $p_{1/2}$ components is more complicated to justify.

The considered phase shift modification is beyond the simplistic PWBA discussed in this work. The question can be asked how realistic is such a modification, which we leave here as an opened question to reaction theory.

2. Suppression of $p_{3/2}$ above $E_T = 1$ MeV

The other possible explanation of the experimental asymmetry function, which naturally stems from Eq. (18) is connected with modification of the high-energy tail of the $p_{3/2}$ resonance. To check such possibility we cut off the high energy $p_{3/2}$ tail via multiplication the $W_{3/2,1}$ population probabilities by Fermi function with energy parameter 1.3 MeV and width parameter 0.15 MeV. The results of calculations are shown in Fig. 17. There is good qualitative agreement at once and also a quantitative agreement with the data may be achieved by small variations of the phase shifts

$$\begin{aligned} \delta_{s_{1/2}} &\to \delta_{s_{1/2}} + 0.05\pi\,, \\ \delta_{s_{1/2}} &\to \delta_{s_{1/2}} + 0.1\pi\,. \end{aligned} \tag{23}$$

Such a suppression of the high-energy tail of the $p_{3/2}$ resonance may find a natural explanation as a threshold effect in the ^{7}He continuum. Indeed, the asymmetry function $R^{(bf)}$ is changing sign at around $E_T = 1.5$ MeV, which is suspiciously close to the ^{6}He(2^+)+n channel threshold at $E_T = 1.8$ MeV. To take this effect into account we need a coupled-channel calculations. Example of such calculations is shown in Fig. 8, where a strong suppression of the ^{6}He(0^+)+n channel population is found around the ^{6}He(2^+)+n threshold energy. We find this possibility the best candidate for reasonable explanation of experimental observations.

3. $s_{1/2}$ resonant state in ^{7}He

One more possible explanation of the experimental asymmetry function, which naturally stems from Eq. (18) is modification of the $s_{1/2}$ continuum component, which can be connected with $s_{1/2}$ resonance somewhere in ^{7}He continuum. The data interpretation in these terms was proposed in Ref. [5]. For this interpretation the R-matrix parameterization was used providing the phase shift

$$\delta_{s_{1/2}}(E_T) = \arctan\left[\frac{S_{s_{1/2}}\, k'}{4M_{tp} r_{\rm ch}(E_r - E_T)}\right] - k' r_{\rm ch}. \tag{24}$$

The first term here is R-matrix resonance phase shift parametrization for the s wave and the second term is just a hard-sphere-scattering phase shift. The calculation results

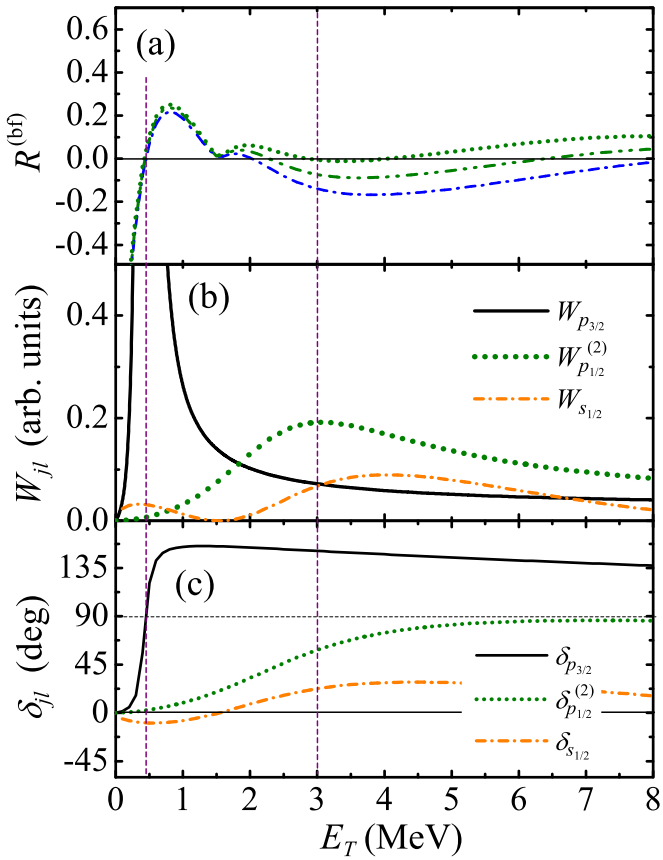

FIG. 18. Asymmetry for $\{s_{1/2}, p_{1/2}, p_{3/2}\}$ interference in PWBA model with single-channel scattering states in the p-wave channels, but with resonant contribution in the $s_{1/2}$ channel: (a) asymmetry function; (b) population probabilities; (c) phase shifts.

with $E_r = 2.0$ MeV, $r_{\rm ch} = 4.5$ fm, $S_{s_{1/2}} = 1.3$ and with s-wave T matrix calculated on-shell are shown in Fig. 18. The resonance width, which can be formally associated with such parametrization is $\Gamma = S_{s_{1/2}} k' r_{\rm ch} = 2$ MeV. Qualitatively reasonable description of the observed asymmetry can be achieved.

This interpretation is based on two assumptions: (i) the off-shell interpolation of the elastic cross section induced by Eq. (24) was assumed to be trivial; the authors of Ref. [5] followed Ref. [50] where the s-wave off-shell interpolation is just constant. (ii) The parameters in the R-matrix expression Eq. (24) can be interpreted as actual resonance properties of the ^{7}He continuum.

Concerning these assumptions we can comment the following:

(i) The off-shell interpolation of the s-wave T matrix is not constant even in the simple potential model. It was shown by direct calculation in Fig. 9 that the off-shell modification of the T-matrix amplitudes can be as large as factor 2–3 both up and down depending on particular properties of the ^{7}He s-wave interaction.

(ii) A resonance in s wave (in contrast with virtual state) can be obtained only in the coupled-channel formulation of the scattering problem. For such formulation the s-wave pole can arise due to coupling with resonant state in some, otherwise closed, channel. We performed the phenomenological studies within coupled-channel model trying to find the situation, which can lead to phase shift behavior analogous to the one shown in Fig. 18. It was possible, but the deduced resonance properties of the continuum were found to be very different: $E_r \approx 6.5$ MeV and $\Gamma \approx 6$ MeV. This is the issue which is very familiar to practitioners of the R-matrix studies: for broad states the R-matrix parameters can be not easy to relate to physical observables. The s-wave continuum just appeared especially weird in this sense.

(iii) In the coupled-channel model the off-shell behavior of the T matrix can be straightforwardly obtained. The results of such calculations are shown in Fig. 19. One may see that the off-shell behavior in such a model is complicated and qualitatively different from the on-shell behavior. So, if we really deal with the resonant state in s wave, the T matrix should be only computed: there is no way to infer it from the on-shell (elastic) scattering T matrix.

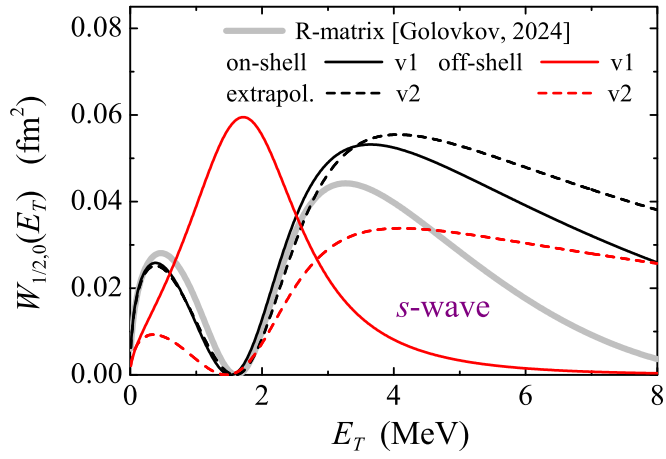

FIG. 19. The population probabilities Eq. (12) presuming existence of a resonant s-wave state are calculated off shell at $\theta_{\rm c.m.} = 8°$, and extrapolated from the on-shell value by Eq. (16). The R-matrix-parameterized value used in Ref. [5] is shown by thick solid gray curve. Black solid and dashed curves shows two versions of the coupled-channel calculations practically coinciding with the latter on shell at $E_T \lesssim 3$ MeV.

Thus, the interpretation proposed in Ref. [5] is phenomenologically possible as off-shell T-matrix parametrization describing the data, but this interpretation can not be unambiguously related to real physics of the ^{7}He continuum described by the on-shell T matrix.

B. Correlations around the ^{7}He g.s.

For the energy range around the ^{7}He g.s. the angular distribution for the ^{6}He -n relative motion can be reconstructed. We make it in the ^{7}He c.m.s. frame with $Z||\mathbf{q}_2$, where the correlation pattern is most prominent in the PWBA model. The data integrated over the $E_T = 0.2$–0.6 MeV range is shown in

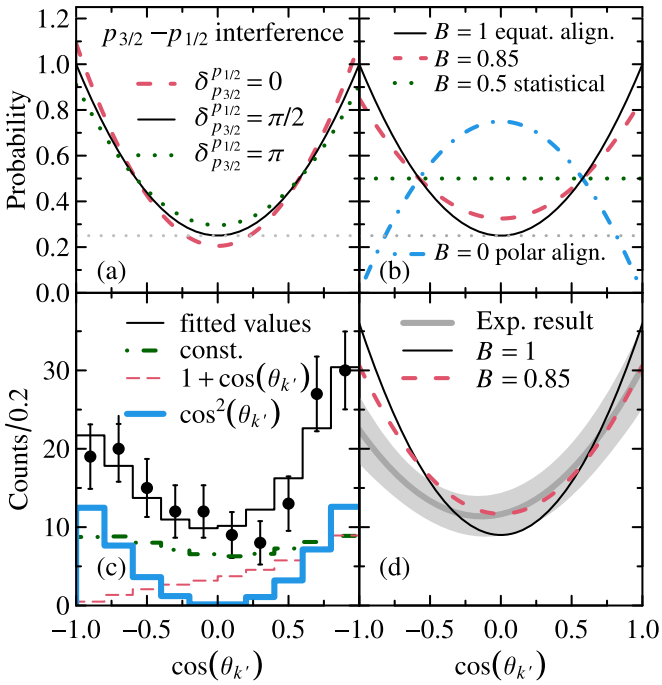

FIG. 20. Angular distributions for the ^{7}He g.s. decay, see Eq. (13). (a) Theoretical angular distribution for the case of $p_{3/2}$-$p_{1/2}$ mixing and complete equatorial alignment $B=1$ for the $p_{3/2}$ amplitude; average relative weight of $p_{1/2}$ is around 10^{-3}. (b) Distributions for pure $p_{3/2}$ state with different alignment B values. (c) Experimental data are shown by circles. The solid histogram shows the result of fit based on Eq. (25); other histograms show contributions of individual terms of (25). (d) Comparison of the distribution obtained from the regression analysis with results of panel (b) shows that a very high alignment is required with confident limit $B > 0.85$.

Fig. 20(c). For the ^{7}He g.s. the description of the angular distribution can be confidently attributed to the $\{s_{1/2}, p_{1/2}, p_{3/2}\}$ interference. Then the whole distribution should be general parabolic shape

$$\frac{dW}{dx} = c_0\frac{1}{2} + c_1\frac{x+1}{2} + c_2\frac{3x^2}{2}, \quad x=\cos(\theta_{k'}). \qquad (25)$$

The distortions of individual terms from Eq. (25) by the experimental setup were studied by using the MC procedure and we may see in Fig. 20(c) that these distortions are modest.

For the pure $p_{3/2}$ the PWBA model Eq. (13) predicts the expressed parabolic profile with hill-to-valley ratio equal 4, see Figs. 20(a), 20(b), 20(d) black solid curve. Let us discuss meaning of this fact and whether some additional information could be extracted from this distribution.

Some asymmetry can be found in the distribution Fig. 20(c). However, this asymmetry is actually difficult to relate to physics of the experiment. The integrated asymmetry effect connected with $p_{3/2}$-$s_{1/2}$ interference at the ^{7}He $p_{3/2}$ g.s. is quite small because asymmetry is changing sign around the $p_{3/2}$ resonant energy and the observed small value is result of fine compensation of large values from below and from above of the resonance. Figure 21 shows how this effect depends on the integration range. It is clear that in any experiment, where the energy resolution is lower than the width of the ^{7}He g.s. such an asymmetry actually shows the integration energy range, which we can afford because of resolution and statistics. It can be also found from Fig. 21 that there is large sensitivity of the integrated asymmetry value on the phase convention. Potentially, this property can be used to determine the phase convention experimentally. At the moment the quality of the data is not sufficient (the error bars shown in this plot are pure statistical, the actual uncertainty is larger). The dependence of the measured asymmetry on the experimental resolution is further elaborated in Fig. 22. Again we can find that potentially, the asymmetry function can be used to determine the phase convention experimentally. However, at the moment the comparison of Fig. 22 can lead only to qualitative conclusions as the CM spectrum has good enough resolution, but low-statistics data with large error bars, while the statistically reliable MM spectrum is spoiled by the low-energy resolution. Another aspect of the angular distributions in Fig. 20 is connected with $p_{3/2}$-$p_{1/2}$ interference and $p_{3/2}$ alignment properties.

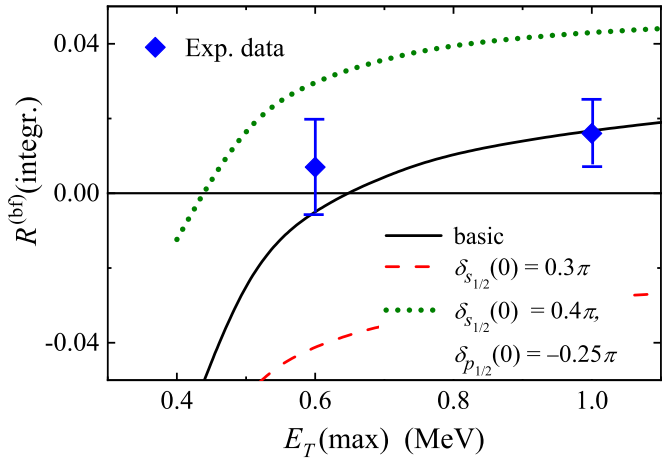

FIG. 21. The asymmetry function integrated in the range $E_T = \{0.2, E_T(\max)\}$. The basic case is obtained from green dotted curve from Fig. 17. The other two cases are obtained by phase modification as in Eq. (22).

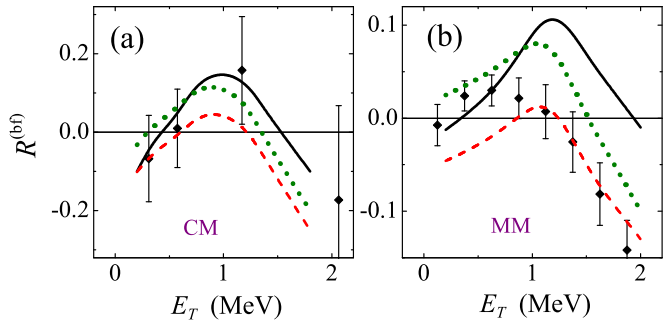

FIG. 22. The asymmetry function taking into account energy resolution is compared to the data. For the CM spectrum (a) the resolution is ≈0.2 MeV FWHM, and MM spectrum (b) the resolution is ≈0.62 MeV. The curves are the same as in Fig. 21.

The $p_{3/2}$-$p_{1/2}$ interference averaged over the energy integration range is illustrated in Fig. 20(a). The effect is small, whatever relative $p_{3/2}$-$p_{1/2}$ phase is assumed. Actually we expect this phase close to $\pi/2$ at the resonance position, and therefore small interference effects anyhow. So, here no sensitivity is found and no information can be extracted.

Situation with alignment is more interesting. Among configurations $p_{3/2}$, $p_{1/2}$, and $s_{1/2}$ only the $p_{3/2}$ one may be spin aligned. It is convenient to discuss the $p_{3/2}$ alignment in terms of the alignment coefficient

$$B = \frac{W_{M=\pm 1/2}}{W_{M=\pm 1/2} + W_{M=\pm 3/2}}.$$

It is clear that for the pure $p_{3/2}$ configuration, the $B = 0.5$ leads to an isotropic angular distribution (this is case of statistical population of magnetic substates), see Fig. 20(b), green dotted curve. The complete equatorial alignment with $B = 1$ leads to an expressed parabolic concave profile with baseline equal to 0.25, see Fig. 20(b), solid black curve. The polar alignment with $B \approx 0$ leads to parabolic convex profiles. The latter profile is clearly in a strong disagreement with the data. The experimental data Fig. 20(d) clearly requires pure or practically pure equatorial alignment with $B > 0.85$. Pure equatorial alignment is trivially predicted in PWBA or similar models, which can be qualitatively attributed to the single-step (or single-pole) reaction mechanism. So, the observed angular distribution confirming the near-perfect equatorial alignment can be seen as strong support of the applicability of the used theoretical approach.

So, to finalize this point, the observed angular correlations for the ^{7}He g.s. decay provide a strong confirmation for a single-pole single-step reaction mechanism leading to population of ^{7}He ground state. We have shown that the data of this kind, but higher quality can be used to establish solidly the phase convention for $s_{1/2}$-$p_{3/2}$ interference in proximity of ^{7}He ground state.

VIII. OUTLOOK

The results obtained in this work show nice prospects of the discussed correlation method for detailed and precise studies of the ^{7}He continuum. The following issues may be addressed in the forthcoming studies of the system.

(i) The use of the combined mass approach allows to drastically improve the energy resolution of the ^{7}He spectrum. Aiming for an experiment with high statistics, it is possible to derive the ^{7}He g.s. width with precision $\Delta\Gamma \approx 10$–15 keV. The ^{7}He g.s. is well known to be not a single-particle state with the dominant $^6\mathrm{He}(2^+) + n$ configuration with spectroscopic factors varying in different studies in the range 0.35–0.65 (e.g., Refs. [6,7]). The improved width data would allow to elaborate this question.

(ii) The variants of explanation for the asymmetry function formulated in Secs. VII A 1, VII A 2, and VII A 3 are to certain extent connected with the limited character of information provided by asymmetry. This drawback could be overcome in a more sophisticated experiment, where high-quality complete correlation information will be available in a broad energy range. The illustration of the predicted complete correlation pattern is given in Fig. 23. The important aspect of information which is missing in the current data is transition convex-concave for the parabolic component of the ^{6}He-n angular distribution. The corresponding part of the cross section is provided in PWBA as

$$\frac{d^2\sigma^{(2)}}{dE_T\,dx} \propto x^2\, a_{p_{3/2}} \left[a_{p_{3/2}} + 2\sqrt{2}\, a_{p_{1/2}} \cos\left(\delta_{p_{1/2}}^{p_{3/2}}\right)\right], \tag{26}$$

and it is clear that the coefficient at the x^2 term is changing sign in the points providing different information compared to the asymmetry coefficient Eq. (18).

(iii) The limitations on the properties of the $1/2^-$ resonance are obtained in this work are not very restrictive. There are two main reasons: (i) unresolved contribution of the $^6\mathrm{He}(2^+)$-n inelastic channel in the experiment. This issue can be easily resolved in a more accurate design of the experimental setup providing the clear identification of ^{4}He and ^{6}He. (ii) Uncertainty in the population of the s-wave continuum. This issue is more complicated as main qualitative properties of the correlations retain, for example, for tenfold (even 50-fold) reduction of the s-wave continuum population compared to the practically maximal possible contribution used in the current analysis. However, potentially it can also be resolved if the precise data of the type shown in Fig. 23 is available.

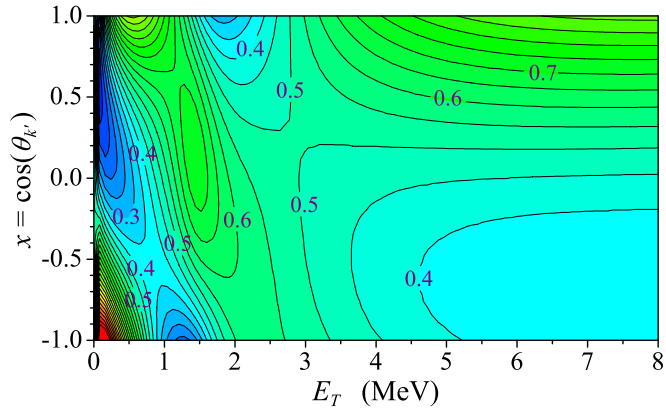

FIG. 23. Complete correlation function $\frac{d^2\sigma}{dE_T dx} / \frac{d\sigma}{dE_T}$ normalized to unit at each E_T value for ^{6}He-n decay. The shown case corresponds to phase prescription of Fig. 17 (green dotted curve), which qualitatively best fits the experimental data shown in Fig. 13(a).

IX. CONCLUSIONS

The ^{7}He continuum states were studied in the ^{2}H(^{6}He, ^{1}H)^{7}He reaction at 29 A MeV. As compared to previous studies in the same reaction [2,3] this experiment

provides higher statistics, higher resolution, and larger excitation energy coverage. The details of the analysis procedure are somewhat different from those published in Refs. [4,5] and there are important differences in interpretation of the data. The interpretation of the data in this work is based on extensive PWBA plus coupled-channel studies. They indicate extreme importance of the careful treatment of the off-shell effects for understanding of the correlation patterns induced in ^{7}He by the (d, p) reaction.

The population cross section for the ^{7}He g.s. is found to be inconsistent with the data [3] obtained at 11.5 A MeV. The c.m.s. angular distributions for the reaction are practically independent on the ^{7}He excitation energy, supporting the same reaction mechanism and the same dominant $\Delta l = 1$ up to $E_T = 8$ MeV.

The ^{7}He $3/2^-$ g.s. properties are established as $E_r = 0.41(2)$ MeV and $\Gamma = 0.14(5)$ keV. Angular distribution for the ^{6}He -n decay of this state can be explained by a strong spin alignment induced by a reaction mechanism. The equatorial spin alignment is a natural feature of the single-step single-pole direct reaction models including PWBA. Thus this fact is a solid confirmation of the robustness of our theoretical considerations.

The correlation information for the higher-lying ^{7}He excitations is available as backward-forward asymmetry for the ^{6}He -n decay in the ^{7}He frame aligned with transferred momentum $\mathbf{q}_2$. The asymmetry function has an expressed profile with three sign-changing points (the first of them is very likely from the data and two others are reliably observed). Such a behavior of this function may be explained by using quite restrictive assumptions and only three such explanations were found:

(i) Strong phase variation (compared to PWBA) due to more complicated reaction mechanism. Possibility of such an interpretation could be confirmed or dismissed by the further advanced reaction theory studies.
(ii) Suppression of $3/2^-$ continuum above $E_T = 1$ MeV. This interpretation gets support from the coupled-channel calculations as a threshold effect in proximity to the ^{6}He(2^+)+n channel threshold.
(iii) The existence of the $s_{1/2}$ resonant state in ^{7}He was declared in Ref. [5] with $E_r \approx 2.0$, $\Gamma \approx 2.0$ MeV. This interpretation is in contradiction with the coupled-channel calculations, which predict extremely strong off-shell effects in this case, providing qualitatively different picture after off-shell correction. No special need for the $s_{1/2}$ resonant state is found in the data analysis of this work.

In all the above scenarios the first excited state of ^{7}He is (quite naturally) $1/2^-$ state with peak positions confined to a range $E_r = 2.2$–3.0 MeV with preferred value around 2.6 MeV. There is an indication on the second $3/2^-$ state in the data with $E_r \approx 4.5$ MeV and the lower resonance energy limit $E_r \gtrsim 3.5$ MeV.

In this work it was demonstrated that the discussed correlation method has the potential to solve the listed burning questions of the ^{7}He continuum. However, it is clear, that the prospective experiments should have higher statistics, higher-energy resolution, and unambiguous identification of the decay channels.

ACKNOWLEDGMENTS

We are grateful to Prof. A. S. Fomichev and Prof. D. E. Lanskoy for important discussions. The research was partly supported within the framework of a scientic program of the Russian National Center for Physics and Mathematics, Topic No. 6 “Nuclear and radiation physics” (2023-2025 stage). We acknowledge the interest and support of this activity from Prof. Yu. Ts. Oganessian, Prof. S. N. Dmitriev, and Prof. S. I. Sidorchuk.

DATA AVAILABILITY

Some of the data that support the findings of this article are openly available [3]. All raw data corresponding to the findings in this article, except data to support Fig. 12(b) are not publicly available upon publication because it is not technically feasible and/or the cost of preparing, depositing, and hosting the data would be prohibitive within the terms of this research project. The data are available from the authors upon reasonable request.

[1] A. A. Korsheninnikov, M. S. Golovkov, A. Ozawa, E. A. Kuzmin, E. Y. Nikolskii, K. Yoshida, B. G. Novatskii, A. A. Ogloblin, I. Tanihata, Z. Fulop, K. Kusaka, K. Morimoto, H. Otsu, H. Petrascu, and F. Tokanai, Phys. Rev. Lett. **82**, 3581 (1999).
[2] M. S. Golovkov, A. A. Korsheninnikov, I. Tanihata, D. D. Bogdanov, M. L. Chelnokov, A. S. Fomichev, V. A. Gorshkov, Y. T. Oganessian, A. M. Rodin, S. I. Sidorchuk, S. V. Stepantsov, G. M. Ter-Akopian, R. Wolski, W. Mittig, P. Roussel-Chomaz, H. Savajols, E. A. Kuzmin, E. Y. Nikolskii, B. G. Novatskii, and A. A. Ogloblin, Phys. At. Nucl. **64**, 1244 (2001).
[3] A. H. Wuosmaa, K. E. Rehm, J. P. Greene, D. J. Henderson, R. V. F. Janssens, C. L. Jiang, L. Jisonna, E. F. Moore, R. C. Pardo, M. Paul, D. Peterson, S. C. Pieper, G. Savard, J. P. Schiffer, R. E. Segel, S. Sinha, X. Tang, and R. B. Wiringa, Phys. Rev. C **72**, 061301(R) (2005).
[4] A. A. Bezbakh, M. S. Golovkov, A. S. Denikin, R. Wolski, S. G. Belogurov, D. Biare, V. Chudoba, A. S. Fomichev,

E. M. Gazeeva, A. V. Gorshkov, G. Kaminski, B. R. Khamidullin, M. Khirk, S. A. Krupko, B. Mauyey, I. A. Muzalevskii, W. Piatek, A. M. Quynh, S. I. Sidorchuk, R. S. Slepnev *et al.*, Int. J. Mod. Phys. E **33**, 2450002 (2024).

[5] M. S. Golovkov, A. A. Bezbakh, A. S. Denikin, R. Wolski, S. G. Belogurov, D. Biare, V. Chudoba, E. M. Gazeeva, A. V. Gorshkov, G. Kaminski, B. R. Khamidullin, S. A. Krupko, B. Mauyey, I. A. Muzalevskii, W. Piatek, A. M. Quynh, R. S. Slepnev, A. Swiercz, P. Szymkiewicz, and B. Zalewski, Phys. Rev. C **109**, L061602 (2024).

[6] F. Renzi, R. Raabe, G. Randisi, D. Smirnov, C. Angulo, J. Cabrera, E. Casarejos, T. Keutgen, A. Ninane, J. L. Charvet, A. Gillibert, V. Lapoux, L. Nalpas, A. Obertelli, F. Skaza, J. L. Sida, N. A. Orr, S. I. Sidorchuk, R. Wolski, M. J. G. Borge *et al.*, Phys. Rev. C **94**, 024619 (2016).

[7] H. T. Fortune, Eur. Phys. J. A **54**, 51 (2018).

[8] K. Markenroth, M. Meister, B. Eberlein, D. Aleksandrov, T. Aumann, L. Axelsson, T. Baumann, M. Borge, L. Chulkov, W. Dostal, T. Elze, H. Emling, H. Geissel, A. Grunschloss, M. Hellstrom, J. Holeczek, B. Jonson, J. Kratz, R. Kulessa, A. Leistenschneider *et al.*, Nucl. Phys. A **679**, 462 (2001).

[9] M. Meister, K. Markenroth, D. Aleksandrov, T. Aumann, T. Baumann, M. Borge, L. Chulkov, D. Cortina-Gil, B. Eberlein, T. Elze, H. Emling, H. Geissel, M. Hellstrom, B. Jonson, J. Kratz, R. Kulessa, A. Leistenschneider, I. Mukha, G. Munzenberg, F. Nickel *et al.*, Nucl. Phys. A **700**, 3 (2002).

[10] D. Halderson, Phys. Rev. C **70**, 041603(R) (2004).

[11] F. Skaza, V. Lapoux, N. Keeley, N. Alamanos, E. C. Pollacco, F. Auger, A. Drouart, A. Gillibert, D. Beaumel, E. Becheva, Y. Blumenfeld, F. Delaunay, L. Giot, K. W. Kemper, L. Nalpas, A. Obertelli, A. Pakou, R. Raabe, P. Roussel-Chomaz, J.-L. Sida *et al.*, Phys. Rev. C **73**, 044301 (2006).

[12] L. Canton, G. Pisent, K. Amos, S. Karataglidis, J. P. Svenne, and D. van der Knijff, Phys. Rev. C **74**, 064605 (2006).

[13] N. Ryezayeva, C. Bäumer, A. van den Berg, L. Chulkov, D. Frekers, D. De Frenne, E.-W. Grewe, P. Haefner, E. Jacobs, H. Johanson, Y. Kalmykov, A. Negret, P. von Neumann-Cosel, L. Popescu, S. Rakers, A. Richter, G. Schrieder, A. Shevchenko, H. Simon, and H. Wörtche, Phys. Lett. B **639**, 623 (2006).

[14] T. Myo, K. Kato, and K. Ikeda, Phys. Rev. C **76**, 054309 (2007).

[15] K. Arai and S. Aoyama, Phys. Rev. C **80**, 027301 (2009).

[16] N. Poppelier, L. Wood, and P. Glaudemans, Phys. Lett. B **157**, 120 (1985).

[17] A. A. Wolters, A. G. M. van Hees, and P. W. M. Glaudemans, Phys. Rev. C **42**, 2062 (1990).

[18] J. Wurzer and H. M. Hofman, Phys. Rev. C **55**, 688 (1997), rGM calculations.

[19] P. Navrátil and B. R. Barrett, Phys. Rev. C **57**, 3119 (1998).

[20] H. G. Bohlen, R. Kalpakchieva, A. Blažević, B. Gebauer, T. N. Massey, W. von Oertzen, and S. Thummerer, Phys. Rev. C **64**, 024312 (2001).

[21] W. Mittig, C. E. Demonchy, H. Wang, P. Roussel-Chomaz, B. Jurado, M. Gelin, H. Savajols, A. Fomichev, A. Rodin, A. Gillibert, A. Obertelli, M. D. Cortina-Gil, M. Caama no, M. Chartier, and R. Wolski, Eur. Phys. J A **25**, 263 (2005).

[22] Y. Aksyutina, H. Johansson, T. Aumann, K. Boretzky, M. Borge, A. Chatillon, L. Chulkov, D. Cortina-Gil, U. D. Pramanik, H. Emling, C. Forssén, H. Fynbo, H. Geissel, G. Ickert, B. Jonson, R. Kulessa, C. Langer, M. Lantz, T. LeBleis, A. Lindahl *et al.*, Phys. Lett. B **679**, 191 (2009).

[23] S. C. Pieper, K. Varga, and R. B. Wiringa, Phys. Rev. C **66**, 044310 (2002).

[24] S. Baroni, P. Navrátil, and S. Quaglioni, Phys. Rev. C **87**, 034326 (2013).

[25] T. Myo, R. Ando, and K. Katō, Phys. Rev. C **80**, 014315 (2009).

[26] D. M. Rodkin and Y. M. Tchuvil'sky, Phys. Rev. C **104**, 044323 (2021).

[27] L. Chen, B. Blank, B. Brown, M. Chartier, A. Galonsky, P. Hansen, and M. Thoennessen, Phys. Lett. B **505**, 21 (2001).

[28] T. Al Kalanee, J. Gibelin, P. Roussel-Chomaz, N. Keeley, D. Beaumel, Y. Blumenfeld, B. Fernández-Domínguez, C. Force, L. Gaudefroy, A. Gillibert, J. Guillot, H. Iwasaki, S. Krupko, V. Lapoux, W. Mittig, X. Mougeot, L. Nalpas, E. Pollacco, K. Rusek, T. Roger *et al.*, Phys. Rev. C **88**, 034301 (2013).

[29] M. S. Golovkov, L. V. Grigorenko, A. S. Fomichev, A. V. Gorshkov, V. A. Gorshkov, S. A. Krupko, Y. T. Oganessian, A. M. Rodin, S. I. Sidorchuk, R. S. Slepnev, S. V. Stepantsov, G. M. Ter-Akopian, R. Wolski, A. A. Korsheninnikov, E. Y. Nikolskii, E. A. Kuzmin, B. G. Novatskii, D. N. Stepanov, P. Roussel-Chomaz, and W. Mittig, Phys. Rev. C **76**, 021605(R) (2007).

[30] S. Fortier, E. Tryggestad, E. Rich, D. Beaumel, E. Becheva, Y. Blumenfeld, F. Delaunay, A. Drouart, A. Fomichev, N. Frascaria, S. Gales, L. Gaudefroy, A. Gillibert, J. Guillot, F. Hammache, K. W. Kemper, E. Khan, V. Lapoux, V. Lima, L. Nalpas *et al.*, AIP Conf. Proc. **912**, 3 (2007).

[31] Y. Jaganathen, R. M. I. Betan, N. Michel, W. Nazarewicz, and M. Płoszajczak, Phys. Rev. C **96**, 054316 (2017).

[32] T. Myo and K. Kato, Prog. Theor. Exp. Phys. **2020**, 12A101 (2020).

[33] K. Fossez, J. Rotureau, and W. Nazarewicz, Phys. Rev. C **98**, 061302(R) (2018).

[34] I. A. Mazur, I. J. Shin, Y. Kim, A. I. Mazur, A. M. Shirokov, P. Maris, and J. P. Vary, Phys. Rev. C **106**, 064320 (2022).

[35] A. S. Fomichev, L. V. Grigorenko, S. A. Krupko, S. V. Stepantsov, and G. M. Ter-Akopian, Eur. Phys. J. A **54**, 97 (2018).

[36] A. A. Bezbakh, S. G. Belogurov, D. Biare, V. Chudoba, A. S. Fomichev, E. M. Gazeeva, M. S. Golovkov, A. V. Gorshkov, G. Kaminski, S. A. Krupko, B. Mauyey, I. A. Muzalevskii, E. Y. Nikolskii, Y. L. Parfenova, W. Piatek, A. M. Quynh, A. Serikov, S. I. Sidorchuk, P. G. Sharov, R. S. Slepnev *et al.*, Bull. Russ. Acad. Sci. Phys. **84**, 491 (2020).

[37] A. A. Bezbakh, S. G. Belogurov, R. Wolski, E. M. Gazeeva, M. S. Golovkov, A. V. Gorshkov, G. Kaminski, M. Y. Kozlov, S. A. Krupko, I. A. Muzalevky, E. Y. Nikolskii, E. V. Ovcharenko, R. S. Slepnev, G. M. Ter-Akopian, A. S. Fomichev, P. G. S. V. Chudoba, and V. N. Schetinin, Instrum. Exp. Tech. **61**, 631 (2018).

[38] P. G. Sharov, A. S. Fomichev, A. A. Bezbakh, V. Chudoba, I. A. Egorova, M. S. Golovkov, T. A. Golubkova, A. V. Gorshkov, L. V. Grigorenko, G. Kaminski, A. G. Knyazev, S. A. Krupko, M. Mentel, E. Y. Nikolskii, Y. L. Parfenova, P. Pluchinski, S. A. Rymzhanova, S. I. Sidorchuk, R. S. Slepnev, S. V. Stepantsov *et al.*, Phys. Rev. C **96**, 025807 (2017).

[39] M. S. Golovkov, L. V. Grigorenko, A. S. Fomichev, Y. T. Oganessian, Y. I. Orlov, A. M. Rodin, S. I. Sidorchuk, R. S. Slepnev, S. V. Stepantsov, G. M. Ter-Akopian, and R. Wolski, Phys. Lett. B **588**, 163 (2004).

[40] M. S. Golovkov, L. V. Grigorenko, A. S. Fomichev, S. A. Krupko, Y. T. Oganessian, A. M. Rodin, S. I. Sidorchuk, R. S. Slepnev, S. V. Stepantsov, G. M. Ter-Akopian, R. Wolski, M. G. Itkis, A. S. Denikin, A. A. Bogatchev, N. A. Kondratiev, E. M. Kozulin, A. A. Korsheninnikov, E. Y. Nikolskii, P. Roussel-Chomaz, W. Mittig, R. Palit *et al.*, Phys. Rev. C **72**, 064612 (2005).

[41] S. I. Sidorchuk, A. S. Fomichev, M. S. Golovkov, L. V. Grigorenko, V. A. Gorshkov, A. V. Gorshkov, S. A. Krupko, Y. T. Oganessian, A. M. Rodin, R. S. Slepnev, S. V. Stepantsov, G. M. Ter-Akopian, and R. Wolski, Nucl. Phys. A **840**, 1 (2010).

[42] S. I. Sidorchuk, A. A. Bezbakh, V. Chudoba, I. A. Egorova, A. S. Fomichev, M. S. Golovkov, A. V. Gorshkov, V. A. Gorshkov, L. V. Grigorenko, P. Jalůvková, G. Kaminski, S. A. Krupko, E. A. Kuzmin, E. Y. Nikolskii, Y. T. Oganessian, Y. L. Parfenova, P. G. Sharov, R. S. Slepnev, S. V. Stepantsov, G. M. Ter-Akopian *et al.*, Phys. Rev. Lett. **108**, 202502 (2012).

[43] D. Tilley, C. Cheves, J. Godwin, G. Hale, H. Hofmann, J. Kelley, C. Sheu, and H. Weller, Nucl. Phys. A **708**, 3 (2002).

[44] F. Beck, D. Frekers, P. von Neumann-Cosel, A. Richter, N. Ryezayeva, and I. Thompson, Phys. Lett. B **645**, 128 (2007).

[45] D. H. Denby, P. A. DeYoung, T. Baumann, D. Bazin, E. Breitbach, J. Brown, N. Frank, A. Gade, C. C. Hall, J. Hinnefeld, C. R. Hoffman, R. Howes, R. A. Jenson, B. Luther, S. M. Mosby, C. W. Olson, W. A. Peters, A. Schiller, A. Spyrou, and M. Thoennessen, Phys. Rev. C **78**, 044303 (2008).

[46] Z. Cao, Y. Ye, J. Xiao, L. Lv, D. Jiang, T. Zheng, H. Hua, Z. Li, X. Li, Y. Ge, J. Lou, R. Qiao, Q. Li, H. You, R. Chen, D. Pang, H. Sakurai, H. Otsu, M. Nishimura, S. Sakaguchi *et al.*, Phys. Lett. B **707**, 46 (2012).

[47] A. Sitenko, Sov. Phys. Usp. **2**, 195 (1959).

[48] I. Shapiro, Nucl. Phys. **28**, 244 (1961).

[49] P. Fröbrich and R. Lipperheide, *Theory of Nuclear Reactions* (Clarendon Press, Oxford, 1996).

[50] H. Fuchs, H. Homeyer, H. Oeschler, R. Lipperheide, and K. Möhring, Nucl. Phys. A **196**, 286 (1972).

[51] L. V. Grigorenko, N. B. Shulgina, and M. V. Zhukov, Phys. Rev. C **102**, 014611 (2020).

[52] S. Sack, L. C. Biedenharn, and G. Breit, Phys. Rev. **93**, 321 (1954).

[53] B. S. Cooper and J. Eisenberg, Nucl. Phys. A **114**, 184 (1968).

[54] D. Brink, Phys. Lett. B **40**, 37 (1972).

[55] A. H. Wuosmaa, J. P. Schiffer, K. E. Rehm, J. P. Greene, D. J. Henderson, R. V. F. Janssens, C. L. Jiang, L. Jisonna, J. C. Lighthall, S. T. Marley, E. F. Moore, R. C. Pardo, N. Patel, M. Paul, D. Peterson, S. C. Pieper, G. Savard, R. E. Segel, R. H. Siemssen, X. D. Tang *et al.*, Phys. Rev. C **78**, 041302(R) (2008).